HERTA: A High-Efficiency and Rigorous Training Algorithm for Unfolded Graph Neural Networks

Anonymous Author(s)
Affiliation
Address
email

Abstract

As a variant of Graph Neural Networks (GNNs), Unfolded GNNs offer enhanced interpretability and flexibility over traditional designs. Nevertheless, they still suffer from scalability challenges when it comes to the training cost. Although many methods have been proposed to address the scalability issues, they mostly focus on per-iteration efficiency, without worst-case convergence guarantees. Moreover, those methods typically add components to or modify the original model, thus possibly breaking the interpretability of Unfolded GNNs. In this paper, we propose HERTA: a High-Efficiency and Rigorous Training Algorithm for Unfolded GNNs that accelerates the whole training process, achieving a nearly-linear time worst-case training guarantee. Crucially, HERTA converges to the optimum of the original model, thus preserving the interpretability of Unfolded GNNs. Additionally, as a byproduct of HERTA, we propose a new spectral sparsification method applicable to normalized and regularized graph Laplacians that ensures tighter bounds for our algorithm than existing spectral sparsifiers do. Experiments on real-world datasets verify the superiority of HERTA as well as its adaptability to various loss functions and optimizers.

1 Introduction

Graph Neural Networks (GNNs) have become a powerful modern tool for handling graph data because of their strong representational capabilities and ability to explore the relationships between data points [22, 2, 42]. Like many deep learning models, GNNs are generally designed by heuristics and experience, which makes analyzing and understanding them a difficult task. *Unfolded GNNs* [45] are a type of GNNs that are rigorously derived from an optimization problem, which makes their inductive bias and training dynamics easier to interpret.

Despite their enhanced interpretability, training unfolded models can be extremely expensive, especially when the graph is large and (relatively) dense. This issue can come from two aspects:

1) *Slow iterations*: in every iteration the whole graph must be fed into the model, and the interactive nature of graphs prevents trivially utilizing techniques like mini-batch training;
2) *Slow convergence*: the training convergence rate is related to the connectivity of the graph and the well-conditionedness of the node features, and the model converges slowly when the data is ill-conditioned.

Many methods have been proposed to address the high cost of training unfolded models [5, 7, 47, 14, 16, 20], primarily by using graph sampling to enable mini-batch training schemes that reduce the per-iteration cost (Issue 1). However, these approaches typically require distorting the underlying optimization objective explicitly or implicitly, thus diminishing the rigorous and interpretable nature of Unfolded GNNs. Moreover, existing works have mostly focused on per-iteration efficiency, while

Submitted to the Mathematics of Modern Machine Learning Workshop at NeurIPS 2024. Do not distribute.

the convergence rate of the optimization in training Unfolded GNNs (Issue 2) remains un-addressed, leading to methods that are not robust to ill-conditioned data.

We propose HERTA: a High-Efficiency and Rigorous Training Algorithm for Unfolded GNNs, which is an algorithmic framework designed to address both Issues 1 and 2, while at the same time preserving the rigorous and interpretable nature of Unfolded GNNs. Unlike many existing methods that require changing the GNN model or defining a new objective, HERTA converges to the optimum of the original training problem, and thus preserves the interpretability of the unfolded models. Moreover, HERTA uses a specialized preconditioner to ensure fast linear convergence to the optimum, requiring only a logarithmic number of passes over the data. We show empirically that HERTA can be used to accelerate training for a variety of GNN objectives, as an extension of popular optimization techniques.

A key novelty of our algorithm lies in the construction of a preconditioner for the GNN objective, which accelerates the convergence rate. To construct this preconditioner, we design a spectral sparsification method for approximating the squared inverse of a normalized and regularized Laplacian matrix, by relying on an extension of the notion of effective resistance to overcome the limitations of existing graph sparsification tools. Below, we present an informal statement of our main result.

Theorem 1.1 (Informal version of Theorem 5.1)**.** *HERTA solves the λ-regularized Unfolded GNN objective* (4.2) *with n nodes, m edges and d-dimensional node features to within accuracy ϵ in time $\tilde{O}\left((m+nd)\left(\log\frac{1}{\epsilon}\right)^2+d^3\right)$ as long as the number of large eigenvalues of the graph Laplacian is $O(n/\lambda^2)$.*

In practice, the node feature dimensionality d is generally much smaller than the graph size m, in which case, the running time of HERTA is $\tilde{O}\left((m+nd)\left(\log\frac{1}{\epsilon}\right)^2\right)$. Notice that to describe a typical graph dataset with m edges, n nodes and d-dimensional node features, we need at least $O(m+nd)$ float or integer numbers. This shows the essential optimality of HERTA: its running time is of the same magnitude as reading the input data (up to logarithm factors).

The condition that the graph Laplacian has $O(n/\lambda^2)$ large eigenvalues is not strictly necessary; it is used here to simplify the time complexity (see Theorem 5.1 for the full statement). This condition is also not particularly restrictive, since in most practical settings the GNN parameter λ is chosen as an absolute constant. At the same time, it is natural that the complexity of training a GNN depends on the number of large eigenvalues in the graph Laplacian, since this quantity can be interpreted as the effective dimension in the Laplacian energy function (4.1) used to define the Unfolded GNN (see more discussion in Section 5).

Outline. The paper is organized as follows. In Section 2 we introduce related work. In Section 3 we introduce the mathematical notation and concepts used in this paper. We define our problem setting in Section 4. In Section 5 we present and analyze our algorithm HERTA, and introduce the techniques that are used in proving the main result. We conduct experiments on real-world datasets and show the results in Section 6. Finally, we conclude with some potential future directions in Section 7.

2 Related Work

Unfolded Graph Neural Networks. Unlike conventional GNN models, which are designed mainly by heuristics, the forward layers of Unfolded GNNs are derived by explicitly optimizing a graph-regularized target function [48, 45, 26, 25, 46, 50, 1]. This optimization nature of Unfolded GNNs allows developing models in a more interpretable and controllable way. The presence of an explicit optimization problem allows designers to inject desired properties into the model and better understand it. This approach has been used to overcome known GNN issues such as over-smoothing [30, 24, 44] and sensitivity towards spurious edges [51, 49].

Efficient Graph Neural Network Training. In order to address the scalability issue of GNNs, many techniques have been proposed. There are two major directions in the exploration of the solutions of this issue. The first direction is to adopt sampling methods. These methods include node-wise sampling [18], layer-wise sampling [6] and subgraph-wise sampling [7, 20]. The second direction is to utilize embeddings from past iterations to enhance current iterations and to obtain more accurate representation with mini-batches and fewer forward layers [16, 14, 43].

As we indicated in Section 1, all of the above methods aim at addressing Issue 1 (*Slow Iterations*), and none of them achieves a worst-case convergence guarantee without affecting the underlying GNN model. In contrast, HERTA addresses both Issue 1 and also Issue 2 (*Slow Convergence*), and possesses a theoretical guarantee on the training convergence rate while preserving the original target model.

Matrix Sketching and Subsampling. Our techniques and analysis are closely related to matrix sketching and subsampling, which are primarily studied in the area of Randomized Numerical Linear Algebra (RandNLA, [41, 15, 27, 29]). Given a large matrix, by sketching or sampling we compress it to a much smaller matrix with certain properties preserved, thus accelerating the solution by conducting expensive computations on the smaller matrix. This type of methods lead to improved randomized algorithms for tasks including low rank approximation [17, 10, 8], linear system solving [32, 13], least squares regression [33, 28] and so on [9]. Our usage of these methods includes constructing spectral sparsifiers of graphs, obtained by edge subsampling [35, 36, 23], which are central in designing fast solvers for Laplacian linear systems [39, 21, 31].

3 Preliminaries

For a vector $\boldsymbol{x}$, we denote its ℓ_2 norm as $\|\boldsymbol{x}\|$. We use $\mathrm{diag}(\boldsymbol{x})$ to denote diagonalization of $\boldsymbol{x}$ into a matrix. For a matrix $\boldsymbol{M}$, we use $\|\boldsymbol{M}\|_{\mathcal{F}}$ and $\|\boldsymbol{M}\|$ to denote its Frobinius norm and operator norm. Let $\sigma_{\max}(\boldsymbol{M})$ and $\sigma_{\min}(\boldsymbol{M})$ be the largest and smallest singular value of $\boldsymbol{M}$ respectively, we denote its condition number as $\kappa(\boldsymbol{M}) = \frac{\sigma_{\max}(\boldsymbol{M})}{\sigma_{\min}(\boldsymbol{M})}$. We use $\mathrm{nnz}(\boldsymbol{M})$ to denote the number of non-zero entries of $\boldsymbol{M}$. For two positive semidefinite (PSD) matrices $\boldsymbol{\Sigma}$ and $\widetilde{\boldsymbol{\Sigma}}$, if there exists $\epsilon \in (0,1)$ such that$(1-\epsilon)\widetilde{\boldsymbol{\Sigma}} \preceq \boldsymbol{\Sigma} \preceq (1+\epsilon)\widetilde{\boldsymbol{\Sigma}}$, then we say $\boldsymbol{\Sigma} \approx_\epsilon \widetilde{\boldsymbol{\Sigma}}$, where $\preceq$ refers to Loewner order. We use $\boldsymbol{\delta}_u$ to denote a vector with u-th entry equal to 1 and all other entries equal to 0. We also use $\delta_{u,v}$ to represent the v-th entry of $\boldsymbol{\delta}_u$, i.e. $\delta_{u,v} = \begin{cases} 1 & u = v \\ 0 & u \neq v \end{cases}$.

For a function $\ell : \mathbb{R}^d \to \mathbb{R}$ that is bounded from bottom, a point $\boldsymbol{w}_0$ is called a solution of ℓ with ϵ error rate if it satisfies $\ell(\boldsymbol{w}_0) \leq (1+\epsilon)\ell^*$ where $\ell^* = \inf_{\boldsymbol{w}} \ell(\boldsymbol{w})$.

We adopt big-O notations in the time complexity analysis. Moreover, we use the notation $\tilde{O}(\cdot)$ to hide polynomial logarithmic factors of the problem size. As an example, $O(\log(n))$ can be expressed as $\tilde{O}(1)$.

For a matrix $\boldsymbol{\Pi} \in \mathbb{R}^{s\times n}$, we call it a Gaussian sketch if its entries are i.i.d. $\mathcal{N}(0, 1/s)$ random variables. For a diagonal matrix $\boldsymbol{R} \in \mathbb{R}^{n\times n}$, we call it a diagonal Rademacher matrix if its entries are i.i.d. Rademacher random variables. See Appendix A for more detailed introductions.

4 Problem Setting

Throughout this paper, we consider a graph $\mathcal{G}$ with n nodes and m edges. We denote its adjacency matrix by $\boldsymbol{A} \in \mathbb{R}^{n\times n}$, degree matrix by $\boldsymbol{D} = \mathrm{diag}(\boldsymbol{A}\mathbf{1}) \in \mathbb{R}^{n\times n}$, where $\mathbf{1} \in \mathbb{R}^n$ is a vector with all entries equal to 1, and Laplace matrix (or Laplacian) by $\boldsymbol{L} = \boldsymbol{D} - \boldsymbol{A} \in \mathbb{R}^{n\times n}$. We also use the normalized adjacency $\hat{\boldsymbol{A}} = \boldsymbol{D}^{-1/2}\boldsymbol{A}\boldsymbol{D}^{-1/2}$ and normalized Laplacian $\hat{\boldsymbol{L}} = \boldsymbol{I} - \hat{\boldsymbol{A}}$. Notice that we assume there's a self-loop for each node to avoid 0-degree nodes, which is commonly ensured in GNN implementations [22, 18], and therefore $\boldsymbol{D}^{-1/2}$ always exists. We also use $\boldsymbol{B} \in \mathbb{R}^{m\times n}$ to represent the incidence matrix of graph $\mathcal{G}$, that is, if the i-th edge in $\mathcal{G}$ is (u_i, v_i), then the i-th row of $\boldsymbol{B}$ is $\boldsymbol{\delta}_{u_i} - \boldsymbol{\delta}_{v_i}$ (the order of u_i and v_i is arbitrary). It is not hard to see that $\boldsymbol{L} = \boldsymbol{B}^\top\boldsymbol{B}$.

We also assume that for each node u in the graph, there is a feature vector $\boldsymbol{x}_u \in \mathbb{R}^d$, and a label vector[1] $\boldsymbol{y}_u \in \mathbb{R}^c$ attached with it. Let $\boldsymbol{X} \in \mathbb{R}^{n\times d}$ and $\boldsymbol{Y} \in \mathbb{R}^{n\times c}$ be the stack of $\boldsymbol{x}_i$-s and $\boldsymbol{y}_i$-s. We assume $n \geq \max\{d, c\}$ and $\boldsymbol{X}$ and $\boldsymbol{Y}$ are both column full rank.

The Unfolded GNN we consider in this paper is based on TWIRLS [46], which is defined by optimizing the following objective (called the "energy function"):

$$E(\boldsymbol{Z}; \boldsymbol{W}) := \frac{\lambda}{2}\mathrm{Tr}\left(\boldsymbol{Z}^\top\hat{\boldsymbol{L}}\boldsymbol{Z}\right) + \frac{1}{2}\left\|\boldsymbol{Z} - f(\boldsymbol{X}; \boldsymbol{W})\right\|_{\mathcal{F}}^2. \tag{4.1}$$

[1]We allow the label to be a vector to make the concept more general. When labels are one-hot vectors, the task is a classification task, and when labels are scalars, it is a regression task.

Here $\boldsymbol{Z} \in \mathbb{R}^{n\times c}$ is the optimization variable that can be viewed as the hidden state of the model, $\boldsymbol{W}$ is the learnable parameter of the model, and $\lambda > 0$ is a hyper-parameter to balance the graph structure information and node feature information. Note that $f : \mathbb{R}^d \to \mathbb{R}^c$ is a function of $\boldsymbol{X}$ and is parameterized by matrix $\boldsymbol{W}$.

For the model training, given a loss function $\ell : \mathbb{R}^{n\times c} \times \mathbb{R}^{n\times c} \to \mathbb{R}$, the training of TWIRLS can be represented by the following bi-level optimization problem

$$\boldsymbol{W}^* \in \arg\min_{\boldsymbol{W}\in\mathbb{R}^{d\times c}} \ell\left[\boldsymbol{Z}^*(\boldsymbol{W}); \boldsymbol{Y}\right] \tag{4.2}$$

$$\text{s.t.} \quad \boldsymbol{Z}^*(\boldsymbol{W}) \in \arg\min_{\boldsymbol{Z}\in\mathbb{R}^{n\times c}} E(\boldsymbol{Z}; \boldsymbol{W}), \tag{4.3}$$

where the solution of inner problem eq.(4.3) (i.e. $\boldsymbol{Z}^*(\boldsymbol{W})$) is viewed as the model output. The outer problem eq.(4.2) is viewed as the problem of training.

In [46], the forward process of TWIRLS is obtained by unfolding the gradient descent algorithm for minimizing E given a fixed $\boldsymbol{W}$:

$$\boldsymbol{Z}^{(t+1)} = \boldsymbol{Z}^{(t)} - \alpha\nabla E\left(\boldsymbol{Z}^{(t)}\right) \tag{4.4}$$

$$= (1-\alpha\lambda-\alpha)\boldsymbol{Z}^{(t)} + \alpha\hat{\boldsymbol{A}}\boldsymbol{Z}^{(t)} + \alpha f\left(\boldsymbol{X}; \boldsymbol{W}\right), \tag{4.5}$$

where $\alpha > 0$ is the step size of gradient descent. Notice that we fix $\boldsymbol{W}$ and view E as a function of $\boldsymbol{Z}$. The model output is $\boldsymbol{Z}^{(T)}$ for a fixed iteration number T. When α is set to a suitable value and T is large, it is clear that $\boldsymbol{Z}^{(T)}$ is an approximation of $\boldsymbol{Z}^*$ defined in eq.(4.3).

When $T \to \infty$, the output of TWIRLS converges to the unique global optimum of eq.(4.1), which has a closed form

$$\boldsymbol{Z}^*(\boldsymbol{W}) = \arg\min_{\boldsymbol{Z}} E(\boldsymbol{Z}) = \left(\boldsymbol{I} + \lambda\hat{\boldsymbol{L}}\right)^{-1} f(\boldsymbol{X}; \boldsymbol{W}). \tag{4.6}$$

In this paper, we always assume $T \to \infty$ and thus we focus on the closed-form solution defined by eq.(4.6).

The training problem is then defined as optimizing $\boldsymbol{W}$ to minimize the loss function between the model output $\boldsymbol{Z}^*(\boldsymbol{W})$ and label $\boldsymbol{Y}$, i.e. $\ell : \mathbb{R}^{n\times d} \times \mathbb{R}^{n\times c} \to \mathbb{R}$.

5 Algorithm and Analysis

In this section we present our main algorithm HERTA, give the convergence result and analyze its time complexity. We also introduce our key techniques and give a proof sketch for the main result. To start we introduce the following notion.

Definition 5.1 (Effective Laplacian dimension)**.** *For normalized Laplacian $\hat{\boldsymbol{L}}$ and regularization term $\lambda > 0$, define $n_\lambda := \mathrm{Tr}\left[\hat{\boldsymbol{L}}\left(\hat{\boldsymbol{L}} + \lambda^{-1}\boldsymbol{I}\right)^{-1}\right]$ to be the effective Laplacian dimension of the graph.*

Denote $\{\lambda_i\}_{i=1}^n$ as the eigenvalues of $\hat{\boldsymbol{L}}$. Then the effective Laplacian dimension can be written as $n_\lambda = \sum_i \frac{\lambda_i}{\lambda_i+\lambda^{-1}}$. We can see that n_λ is roughly the number of eigenvalues of $\hat{\boldsymbol{L}}$ which are of order $\Omega(\lambda^{-1})$, i.e., the number of "large eigenvalues" mentioned in Theorem 1.1. It is not hard to see that $n_\lambda \le n$ and $n_\lambda \to n$ as $\lambda \to \infty$.

Intuitively, n_λ represents the number of eigen-directions for which the Laplacian regularizer $\frac{\lambda}{2}\mathrm{Tr}(\boldsymbol{Z}^\top\hat{\boldsymbol{L}}\boldsymbol{Z})$ is large, thus having a significant impact on the energy function (4.1). For the remaining eigen-directions which are less significant, the effect of the regularizer is minimal. This can also be seen from the closed form solution of the model (4.6): when we apply matrix $(\boldsymbol{I} + \lambda\hat{\boldsymbol{L}})^{-1}$ to a vector, the effect of the Laplacian is dominated by the $\boldsymbol{I}$ term if this vector is aligned with a "small" Laplacian eigen-direction (i.e., with an eigenvalue significantly smaller than λ^{-1}), and thus the objective is close to the usual unregularized least squares loss.

Based on the above discussion, it stands to reason that the larger the effective Laplacian dimension n_λ of the graph, the more work we must do during the training to preserve the graph structure of the GNN.

5.1 Main Result

In this subsection, we present our main theoretical result. Before delving into the specific theorem, we first outline the model implementation used in our theoretical analysis. Although we make specific assumptions for this analysis, the experiments (see Section 6) demonstrate that our proposed algorithm is effective in broader settings beyond those considered here.

Principally, the implementation of $f(\boldsymbol{X}; \boldsymbol{W})$ can be arbitrary as long as it can be trained (i.e. computable, smooth, etc.), however, we noticed that in [46], most of the SOTA results are achieved by the implementation $f(\boldsymbol{X}; \boldsymbol{W}) = \boldsymbol{X}\boldsymbol{W}$ where $\boldsymbol{W} \in \mathbb{R}^{d\times c}$. Therefore, hereinafter we focus on this specific implementation.

For the simplicity of analysis, we present our theoretical result based on the mean squared error (MSE) loss defined as $\ell(\boldsymbol{Z}, \boldsymbol{Y}) := \frac{1}{2}\|\boldsymbol{Z} - \boldsymbol{Y}\|_{\mathcal{F}}^2$. Despite this specific choice in the analysis, we empirically show in Section 6 that our algorithm also works for cross entropy (CE) loss, which is the most commonly used loss function for node classification tasks.

Under MSE loss, we can decompose the loss into sub-losses for each class, i.e. $\ell\left[\boldsymbol{Z}^*(\boldsymbol{W}); \boldsymbol{Y}\right] = \sum_{i=1}^{c} \ell_i(\boldsymbol{w}_i; \boldsymbol{y}_i)$, where $\boldsymbol{w}_i$ and $\boldsymbol{y}_i$ are the i-th column of $\boldsymbol{W}$ and $\boldsymbol{Y}$ respectively. In the following analysis, we will mostly focus on each ℓ_i. Moreover, we fix $\boldsymbol{y}_i$, and view ℓ_i as a function of $\boldsymbol{w}_i$.

Theorem 5.1 (Main result)**.** *For any $\epsilon > 0$, with a proper step size η, number of iterations T and constant $K > 0$, Algorithm 1 finds a solution $\hat{\boldsymbol{W}} \in \mathbb{R}^{d\times c}$ in time*

$$\tilde{O}\left((m + nd)\, c \left(\log\frac{1}{\epsilon}\right)^2 + n_\lambda \lambda^2 d + d^3\right) \tag{5.1}$$

such that with probability $1 - \frac{1}{n}$, $\ell\left[\boldsymbol{Z}^*(\hat{\boldsymbol{W}}); \boldsymbol{Y}\right] \le (1+\epsilon)\cdot \ell^*$, where $\ell^* := \min_{\boldsymbol{W}} \ell\left[\boldsymbol{Z}^*\left(\boldsymbol{W}; \boldsymbol{Y}\right)\right]$.

Notice that if we assume $n_\lambda = O(n/\lambda^2)$, then $\tilde{O}(n_\lambda \lambda^2 d) = \tilde{O}(nd)$. By further assuming the number of classes $c = O(1)$, we recover the bound given by Theorem 1.1.

Before heading into the details of HERTA (Algorithm 1), in next subsection we first analyze the original (standard) implementation of training TWIRLS and point out the efficiency bottlenecks. We then introduce the key techniques and methods we need to prove our main result. Finally we present our main algorithm HERTA, and give a proof sketch for Theorem 5.1.

5.2 Analysis of TWIRLS Training

In this subsection, we introduce the framework that we use to analyze the complexity of TWIRLS training. We also provide a complexity analysis of the original implementation used in [46].

As noted in Section 4, the whole optimization problem can be viewed as a bi-level optimization problem, where the inner-problem eq.(4.3) approximates the linear system solver $\left(\boldsymbol{I} + \lambda\hat{\boldsymbol{L}}\right)^{-1}(\boldsymbol{X}\boldsymbol{w}_i - \hat{\boldsymbol{y}}_i)$, and the outer problem eq.(4.2) uses the linear system solution to approximate the optimal solution of the training loss. When we discuss the solution of outer problems, we treat the solver of the inner problem (linear solver) as a black box. We formally define a linear solver as follows.

Definition 5.2 (Linear solver)**.** *For a positive definite matrix $\boldsymbol{H} \in \mathbb{R}^{n\times n}$ and a real number $\epsilon > 0$, we call $f : \mathbb{R}^n \to \mathbb{R}^n$ a linear solver for $\boldsymbol{H}$ with ϵ error rate if it satisfies*

$$\forall \boldsymbol{u} \in \mathbb{R}^n,\ \left\|f(\boldsymbol{u}) - \boldsymbol{H}^{-1}\boldsymbol{u}\right\|_{\boldsymbol{H}} \le \epsilon \left\|\boldsymbol{H}^{-1}\boldsymbol{u}\right\|_{\boldsymbol{H}}. \tag{5.2}$$

In [46], the outer problem is also solved by standard gradient descent. The gradient of $\ell_i\left(\boldsymbol{w}_i\right)$ is

$$\nabla\ell_i(\boldsymbol{w}_i) = \boldsymbol{X}^\top\left(\boldsymbol{I} + \lambda\hat{\boldsymbol{L}}\right)^{-2}\left(\boldsymbol{X}\boldsymbol{w}_i - \hat{\boldsymbol{y}}_i\right), \tag{5.3}$$

where $\hat{\boldsymbol{y}}_i = (\boldsymbol{I} + \lambda\hat{\boldsymbol{L}})\boldsymbol{y}_i$.

In actual implementation, the matrix inverse is calculated by linear solvers. Suppose that we have a linear solver for $(\boldsymbol{I} + \lambda\hat{\boldsymbol{L}})$ denoted by $\mathcal{S}$, then by embedding it into eq.(5.3) we can obtain the gradient approximation as

$$\widetilde{\nabla\ell_i(\boldsymbol{w}_i)} := \boldsymbol{X}^\top\mathcal{S}\left[\mathcal{S}\left(\boldsymbol{X}\boldsymbol{w}_i - \hat{\boldsymbol{y}}_i\right)\right]. \tag{5.4}$$

The following convergence result can be derived for this approximate gradient descent. See Appendix for the proof.

Lemma 5.1 (Convergence)**.** *If we minimize ℓ_i using gradient descent with the gradient approximation defined in eq.(5.4), where $\mathcal{S}$ is a linear solver of $\boldsymbol{I} + \lambda\hat{\boldsymbol{L}}$ with μ error rate satisfying $\mu \leq \min\left\{\frac{\epsilon^{1/2}}{50\kappa(\boldsymbol{X})\lambda^2}, 1\right\}$, then, to obtain an $\epsilon \in (0,1)$ error rate the outer problem (i.e. ℓ_i), the number of iterations needed is $T = O\left(\kappa \log \frac{1}{\epsilon}\right)$, where $\kappa := \kappa(\boldsymbol{X}^\top(\boldsymbol{I} + \lambda\hat{\boldsymbol{L}})^{-2}\boldsymbol{X})$.*

Based on Lemma 5.1, in Appendix B we provide a detailed analysis of the time complexity of the implementation used by [46]. From this analysis, one can figure out two bottlenecks of the computational complexity for solving TWIRLS: 1) The number of iterations needed for the inner loop is dependent on λ; 2) The number of iterations needed for the outer loop is dependent on the condition number of the outer problem. Our acceleration algorithm is based on the following two observations, which correspond to the aforementioned bottlenecks:

1. The data matrix in the inner loop is a graph Laplacian plus identity. It is possible to solve the linear system defined by this matrix faster by exploiting its structure.
2. A good enough preconditioner can be constructed for the outer iteration using techniques from RandNLA.

5.3 Key Techniques

In this subsection, we introduce the mathematical tools that we will use in the proof of our main result.

SDD Solvers. If a symmetric matrix $\boldsymbol{H} \in \mathbb{R}^{n\times n}$ satisfies

$$\forall 1 \leq k \leq n,\ \ \boldsymbol{H}_{k,k} \geq \sum_{i=1}^{n} |\boldsymbol{H}_{k,i}|\,, \tag{5.5}$$

it is called a symmetric diagonal dominated (SDD) matrix. It has been shown that the linear system defined by sparse SDD matrices can be solved in an efficient way, via a SDD solver [21, 31].

Since $\boldsymbol{I} + \lambda\hat{\boldsymbol{L}}$ is indeed a SDD matrix in our problem, we can apply off-the-shelf SDD solvers. In the following, we use $\mathsf{SSolve}_\epsilon(\boldsymbol{H}, \boldsymbol{u})$ to denote the SDD solver that calculates $\boldsymbol{H}^{-1}\boldsymbol{u}$ with error rate less or equal to ϵ[2]. From Lemma A.1, the time complexity of calculating $\mathsf{SSolve}_\epsilon(\boldsymbol{H}; \boldsymbol{u})$ is $\tilde{O}\left[\mathrm{nnz}(\boldsymbol{H})\right]$. See Appendix A.2 for details.

Fast Matrix Multiplication. For a matrix $\boldsymbol{Q} \in \mathbb{R}^{n\times d}$ where $n > d$, it is known that calculating $\boldsymbol{Q}^\top\boldsymbol{Q}$ takes $O(nd^2)$ time if implemented by brute force. In HERTA, we manage to achieve a faster calculation of $\boldsymbol{Q}^\top\boldsymbol{Q}$ through Subsampled Randomized Hadamard Transformation (SRHT) [37, 41]. The key idea of SRHT is to first apply a randomized Hadamard transformation to the matrix to make the "information" evenly distributed in each row, then uniformly sample the rows of $\boldsymbol{Q}$ to reduce the dimension. In the following, we use $\mathsf{Hadamard}$ to represent the Hadamard transformation, see Appendix A.3 for the definition of $\mathsf{Hadamard}$ as well as a detailed introduction.

5.4 Regularized Spectral Sparsifier

It has been shown that for any connected graph with n nodes, (no matter how dense it is) there is always a sparsified graph with $\tilde{O}\left(\frac{n}{\epsilon^2}\right)$ edges whose Laplacian is an ϵ-spectral approximation of the original graph Laplacian [36]. Although the existence is guaranteed, it is generally hard to construct such a sparsified graph. An algorithm that finds such a sparsified graph is called a spectral sparsifier.

While there has been many existing explorations on constructing spectral sparsifier of a given graph with high probability and tolerable time complexity [35, 36, 23], the setting considered in this paper is different from the standard one: instead of graph Laplacian $\boldsymbol{L}$, the matrix we concern is the normalized and regularized Laplacian $\hat{\boldsymbol{L}} + \lambda^{-1}\boldsymbol{I}$.

[2] Principally, $\mathsf{SSolve}(\boldsymbol{H}; \cdot)$ is a vector function, but for convenience we sometimes also apply it to matrices, in which case we mean applying it column-wisely. We also use the same convention for other vector functions.

At first glance, a spectral sparsifier also works for our problem since $\tilde{\boldsymbol{L}} \approx_\epsilon \hat{\boldsymbol{L}}$ implies $\tilde{\boldsymbol{L}} + \lambda^{-1}\boldsymbol{I} \approx_\epsilon \hat{\boldsymbol{L}} + \lambda^{-1}\boldsymbol{I}$. However, it turns out that it is possible to make the bound even tighter if we take into account the regularization term $\lambda^{-1}\boldsymbol{I}$ here. A similar argument is also made in [4]. We note that the setting explored in [4] is also different from ours: we consider the normalized Laplacian of a graph, which is not a Laplacian of any graph (even allowing weighted edges).

To this end, we propose a new spectral sparsifier that works for $\hat{\boldsymbol{L}} + \lambda^{-1}\boldsymbol{I}$ which is used in our problem. This spectral sparsifier reduces the number of edges to $O\left(\frac{n_\lambda}{\epsilon^2}\log n\right)$, which, as we discussed before, is smaller than $O\left(\frac{n}{\epsilon^2}\log n\right)$ obtained by standard spectral sparsifier.

Lemma 5.2 (Regularized spectral sparsifier)**.** *Let $\hat{\boldsymbol{L}}$ be a (normalized) graph Laplacian with m edges and n nodes. There exists a constant C such that for any $\epsilon > 0$ and $\lambda > 0$, Algorithm 2 outputs a (normalized) graph Laplacian $\tilde{\boldsymbol{L}}$ with n nodes and $O\left(\frac{n_\lambda}{\epsilon^2}\log n\right)$ edges in time $\tilde{O}(m)$, such that $\tilde{\boldsymbol{L}} + \lambda^{-1}\boldsymbol{I} \approx_\epsilon \hat{\boldsymbol{L}} + \lambda^{-1}\boldsymbol{I}$ with probability at least $1 - \frac{1}{2n}$.*

The basic idea behind Lemma 5.2 is to use ridge leverage score sampling for the normalized incidence matrix $\boldsymbol{B}\boldsymbol{D}^{-1/2}$ [10], which reduces the problem to estimating a regularized version of the effective resistance. We modify the existing methods of estimating effective resistance [38] to make it work for the normalized and regularized Laplacian.

Algorithm 1 HERTA: A High-Efficiency and Rigorous Training Algorithm for TWIRLS

Input: $\hat{\boldsymbol{L}}, \boldsymbol{X}, \boldsymbol{Y}$, λ, c, $K > 0$, step size η and number of iteration T.
Set $\beta = \frac{1}{64}$, $s = \frac{Kd}{\beta^2}\log n$, $\mu = \min\left\{\frac{\epsilon^{1/2}}{50\kappa(\boldsymbol{X})\lambda^2}, 1\right\}$ and $\boldsymbol{R} \in \mathbb{R}^{n\times n}$ a diagonal Rademacher matrix;
$\tilde{\boldsymbol{L}} \leftarrow \mathsf{Sparsify}_{\frac{\beta}{3\lambda}}(\hat{\boldsymbol{L}})$ by calling Algorithm 2;
$\boldsymbol{Q} \leftarrow \mathsf{SSolve}_{\frac{\beta}{\sqrt{3}\lambda}}\left(\boldsymbol{I} + \lambda\tilde{\boldsymbol{L}}; \boldsymbol{X}\right)$;
$\boldsymbol{Q}' \leftarrow \mathsf{Hadamard}\left(\boldsymbol{R}\boldsymbol{Q}\right)$;
Subsample s rows of $\boldsymbol{Q}'$ uniformly and obtain $\tilde{\boldsymbol{Q}}$;
$\boldsymbol{P} \leftarrow \tilde{\boldsymbol{Q}}^\top\tilde{\boldsymbol{Q}}$;
$\boldsymbol{P}' \leftarrow \boldsymbol{P}^{-1/2}$;
for $i = 1$ **to** c **do**
  $\hat{\boldsymbol{y}}_i \leftarrow (\boldsymbol{I} + \lambda\hat{\boldsymbol{L}})\boldsymbol{y}_i$, where $\boldsymbol{y}_i$ is the i-th column of $\boldsymbol{Y}$;
  Initialize $\boldsymbol{w}_i^{(0)}$ by all zeros;
  for $t = 1$ **to** T **do**
    $\boldsymbol{u}_i^{(t)} \leftarrow \boldsymbol{X}\boldsymbol{P}'\boldsymbol{w}_i^{(t-1)} - \hat{\boldsymbol{y}}_i$;
    $\boldsymbol{u}_i^{(t)'} \leftarrow \mathsf{SSolve}_\mu\left(\boldsymbol{I} + \lambda\hat{\boldsymbol{L}}; \boldsymbol{u}_i^{(t)}\right)$;
    $\boldsymbol{u}_i^{(t)''} \leftarrow \mathsf{SSolve}_\mu\left(\boldsymbol{I} + \lambda\hat{\boldsymbol{L}}; \boldsymbol{u}_i^{(t)'}\right)$;
    $\boldsymbol{g}_i^{(t)} \leftarrow \boldsymbol{P}'\boldsymbol{X}^\top\boldsymbol{u}_i^{(t)''}$;
    $\boldsymbol{w}_i^{(t)} \leftarrow \boldsymbol{w}_i^{(t-1)} - \eta\boldsymbol{g}_i^{(t)}$;
  end for
end for
Output: $\left\{\boldsymbol{w}_i^{(T)}\right\}_{i=1}^c$.

Algorithm 2 $\mathsf{Sparsify}_\epsilon(\hat{\boldsymbol{L}})$: Regularized Spectral Sparsifier

Input: $\hat{\boldsymbol{L}}, \hat{\boldsymbol{B}}, \lambda$, $C > 0$ and expected error rate ϵ.
Set $k = C\log m$ and $s = \frac{Cn_\lambda\log n}{\epsilon^2}$,and construct Gaussian sketch $\boldsymbol{\Pi}_1 \in \mathbb{R}^{k\times m}, \boldsymbol{\Pi}_2 \in \mathbb{R}^{k\times n}$;
$\boldsymbol{B}_{\mathcal{S}} \leftarrow \mathsf{SSolve}_{2^{1/4}}(\hat{\boldsymbol{L}} + \lambda^{-1}\boldsymbol{I}; (\boldsymbol{\Pi}_1\hat{\boldsymbol{B}})^\top)$;
$\boldsymbol{\Pi}_{\mathcal{S}} \leftarrow \mathsf{SSolve}_{2^{1/4}}(\hat{\boldsymbol{L}} + \lambda^{-1}\boldsymbol{I}; \boldsymbol{\Pi}_2^\top)$;
for $i = 1$ **to** m **do**
  $\tilde{l}_i \leftarrow \|\boldsymbol{B}_{\mathcal{S}}\hat{\boldsymbol{b}}_i\|^2 + \lambda^{-1}\|\boldsymbol{\Pi}_{\mathcal{S}}\hat{\boldsymbol{b}}_i\|^2$, where $\hat{\boldsymbol{b}}_i^\top$ is the i-th row of $\hat{\boldsymbol{B}}$;
end for
$Z \leftarrow \sum_{i=1}^m \tilde{l}_i$;
Subsample s rows of $\hat{\boldsymbol{B}}$ with probabilities $\left\{\tilde{l}_i/Z\right\}_{i=1}^m$ and obtain $\tilde{\boldsymbol{B}}$;
$\tilde{\boldsymbol{L}} \leftarrow \tilde{\boldsymbol{B}}^\top\tilde{\boldsymbol{B}}$;
Output: $\tilde{\boldsymbol{L}}$.

5.5 Main Algorithm

Now we are ready to present our main algorithm HERTA, see Algorithm 1. As mentioned before, HERTA is composed of two major components: constructing a preconditioner matrix $\boldsymbol{P}$ and applying it to the optimization problem. Below we introduce each part.

Constructing the Preconditioner. For the outer problem which can be ill-conditioned, we first precondition it using a preconditioner $\boldsymbol{P} \in \mathbb{R}^{d\times d}$ which is a constant level spectral approximation of

the Hessian, i.e. $\boldsymbol{X}^\top \left(\boldsymbol{I} + \lambda \hat{\boldsymbol{L}}\right)^{-2} \boldsymbol{X}$. We claim that the matrix $\boldsymbol{P}$ constructed inside Algorithm 1 indeed satisfies this property.

Lemma 5.3 (Preconditioner)**.** *Let $\boldsymbol{P}$ be the matrix constructed in Algorithm 1. We have $\boldsymbol{P} \approx_{\frac{1}{2}} \boldsymbol{X}^\top \left(\boldsymbol{I} + \lambda \hat{\boldsymbol{L}}\right)^{-2} \boldsymbol{X}$ with probability at least $1 - \frac{1}{n}$.*

Solving the Outer Problem. After obtaining the preconditioner $\boldsymbol{P}$ which approximates the Hessian by a constant level, we use it to precondition the outer problem and provably reduce the condition number to a constant. With the new problem being well-conditioned, iterative methods (like gradient descent) take much less steps to converge.

Lemma 5.4 (Well-conditioned Hessian)**.** *Let ℓ' be such that $\ell'(\boldsymbol{w}_i) = \ell(\boldsymbol{P}^{-1/2}\boldsymbol{w}_i)$. Suppose for some constant $c_0 \in (0,1)$ we have $\boldsymbol{P} \approx_{c_0} \boldsymbol{X}^\top \left(\boldsymbol{I} + \lambda \hat{\boldsymbol{L}}\right)^{-2} \boldsymbol{X}$, then the condition number of the Hessian of ℓ' is bounded by*

$$\kappa\left(\nabla^2 \ell'\right) \leq (1 + c_0)^2. \tag{5.6}$$

Moreover, if $\boldsymbol{w}'$ is a solution of ℓ' with ϵ error rate, then $\boldsymbol{P}^{-1/2}\boldsymbol{w}'$ is a solution of ℓ with ϵ error rate.

Notice that, the problem ℓ' defined in Lemma 5.4 can be viewed as the original problem ℓ with $\boldsymbol{X}$ being replaced by $\boldsymbol{X}\boldsymbol{P}^{-1/2}$, therefore we can use Lemma 5.1 and obtain the convergence rate of HERTA. With the convergence result and analysis of the running time for each step, we are able to prove Theorem 5.1. See Appendix C.7 for the full proof.

Remark on the Unavoidable λ^2 in Runtime. Notice that λ^2 appears in the time bound given in Theorem 5.1. From the proof in Appendix C.5 we can see that this term originates from the squared inverse of $\boldsymbol{I} + \lambda \hat{\boldsymbol{L}}$. In Appendix D.2, we show that in the worst case even if we approximate a matrix to a very high precision, the approximation rate of the corresponding squared version can still be worse by a factor of the condition number of the matrix, which in our case leads to the unavoidable λ^2 in the runtime.

Remark on Sparsifying the Graph in Each Iteration. Note that in Algorithm 1, we use the complete Laplacian $\hat{\boldsymbol{L}}$ for gradient iterations (i.e., the for-loop), and the graph sampling only occurs when constructing the preconditioner $\boldsymbol{P}$. We note that sampling $\hat{\boldsymbol{L}}$ in the for-loop can lead to extra loss in the gradient estimation, which forces us to sparsify the graph to a very high precision to ensure an accurate enough gradient for convergence. This could result in a suboptimal running time. Moreover, as discussed in Section 1, the current running time bound for HERTA is optimal up to logarithmic factors, which means that there is little to gain from performing extra sampling in for-loops. See Appendix D.3 for a more detailed and quantitative discussion.

6 Experiments

In this section, we verify our theoretical results through experiments on real world datasets. Since for the inner problem we use off-the-shelf SDD solvers, in this section we focus on the outer problem, i.e. the training loss convergence rate. In each setting we compare the training loss convergence rate of TWIRLS trained by our method against that trained by standard gradient descent using exactly the same training hyper-parameters.

Datasets. We conduct experiments on all of the datasets used in the Section 5.1 of [46]: Cora, Citeseer and Pubmed collected by [34], as well as the ogbn-arxiv dataset from the Open Large Graph Benchmark (OGB, 19).

Notice that for Cora, Citeseer and Pubmed, common practice uses the semi-supervised setting where there is a small training set and relatively large validation set. As we are comparing training convergence rate, we find it more comparative to use a larger training set (which makes solving the optimization problem of training more difficult). Therefore, we randomly select 80% of nodes as training set for Cora, Citeseer and Pubmed. For OGB, we use the standard training split.

Due to limited space, we only include the results with $\lambda = 1$ and with datasets Citeseer, Pubmed and ogbn-arxiv in this section, and delay additional results to Appendix F.

6.1 Convergence Rate Comparison Under MSE Loss

In this section, we compare the convergence rate for models trained with MSE loss, which is well aligned with the setting used to derive our theory. We also adopt a variation of HERTA that allows using it on other optimizers and apply it on Adam optimizer. See Figure 1 for the results. Notice that for each figure, we shift the curve by the minimum value of the loss (which is approximated by running HERTA for more epochs) and take logarithm scale to make the comparison clearer.

From the results, it is clear that on all datasets and all optimizers we consider, HERTA converges much faster than standard methods. It generally requires ≤ 10 iterations to get very close to the smallest training loss. This shows that the guarantee obtained in our theoretical results (Theorem 5.1) not only matches the experiments, but also holds when the setting is slightly changed (using other optimizers). Thus, these experimental results verify the universality of HERTA as an optimization framework.

We also conduct extensive experiments with larger λ. See Appendix F for the results. These results verify that even when λ is relatively large, HERTA converges very fast, which suggests that the dominant term in Theorem 5.1 is the $\tilde{O}(m)$ term instead of the $\tilde{O}(n_\lambda \lambda^2 d)$ term.

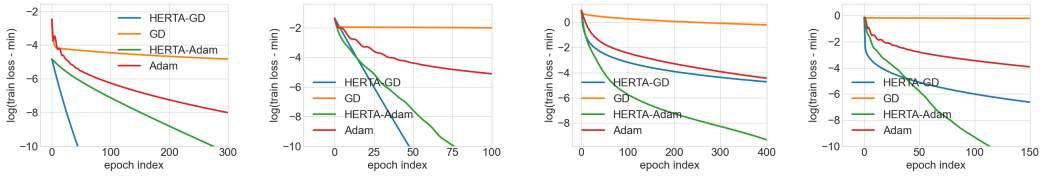

Figure 1: The training loss comparison between HERTA and standard optimizers on MSE loss with $\lambda = 1$. Left: ogbn-arxiv; Right: pubmed.

Figure 2: The training loss comparison between HERTA and standard optimizers on CE loss with $\lambda = 1$. Left: ogbn-arxiv; Right: pubmed.

6.2 Convergence Rate Comparison under Cross Entropy Loss

Note that in the theoretical analysis of Section 5, we focus on the MSE loss. However, for graph node classification tasks, MSE is not the most commonly used loss. Instead, most node classification models use the cross entropy loss. For example, the original TWIRLS paper [46] uses CE loss.

To this end, we also adopt HERTA on training problems with CE loss. See Appendix E for the details of the implementation. The results are displayed in Figure 2. From these results, it is clear that HERTA also significantly speeds up training with CE loss. The results demonstrate that although originally developed on MSE loss, HERTA is not limited to it and have the flexibility to be applied to other type of loss functions.

Remark on the Surprising Effectiveness of HERTA on Cross Entropy Loss. In Section 6.2, we observe that despite not being guaranteed by the theoretical result, HERTA shows a certain degree of universality in that it also works on CE loss. We claim that this phenomenon might originate from the fact the Hessians of TWIRLS under MSE loss and CE loss are very similar. We provide an analysis of the gradient and Hessian of TWIRLS under MSE and CE losses in Appendix D.1. The results show that the gradient under CE loss can be viewed as the gradient under MSE loss with one term being normalized by softmax, and the Hessian under CE loss can be viewed as a rescaled version of the Hessian under MSE loss. These comparisons serve as an explanation of why HERTA works so well with CE loss.

7 Conclusions

In this paper we present HERTA: a High-Efficiency and Rigorous Training Algorithm that solves the problem of training Unfolded GNNs on a graph within a time essentially of the same magnitude as the time it takes to load the input data. As a component of HERTA, we also propose a new spectral sparsifier that works for normalized and regularized graph Laplacian matrices.

Experimental results on real world datasets show the effectiveness of HERTA. Moreover, it is shown that HERTA works for various loss functions and optimizers, despite being derived from a specific loss function and optimizer. This shows the universality of HERTA and verifies that it is ready to use in practice. See Appendix D for further discussions and possible extensions of HERTA.

References

[1] Hongjoon Ahn, Yongyi Yang, Quan Gan, Taesup Moon, and David P Wipf. Descent steps of a relation-aware energy produce heterogeneous graph neural networks. *Advances in Neural Information Processing Systems*, 35:38436–38448, 2022.

[2] Peter W Battaglia, Jessica B Hamrick, Victor Bapst, Alvaro Sanchez-Gonzalez, Vinicius Zambaldi, Mateusz Malinowski, Andrea Tacchetti, David Raposo, Adam Santoro, Ryan Faulkner, et al. Relational inductive biases, deep learning, and graph networks. *arXiv preprint arXiv:1806.01261*, 2018.

[3] Léon Bottou, Frank E. Curtis, and Jorge Nocedal. Optimization methods for large-scale machine learning. *SIAM Rev.*, 60(2):223–311, 2018.

[4] Daniele Calandriello, Alessandro Lazaric, Ioannis Koutis, and Michal Valko. Improved large-scale graph learning through ridge spectral sparsification. In *International Conference on Machine Learning*, pages 688–697. PMLR, 2018.

[5] Jianfei Chen, Jun Zhu, and Le Song. Stochastic training of graph convolutional networks with variance reduction. In Jennifer G. Dy and Andreas Krause, editors, *Proceedings of the 35th International Conference on Machine Learning, ICML 2018, Stockholmsmässan, Stockholm, Sweden, July 10-15, 2018*, volume 80 of *Proceedings of Machine Learning Research*, pages 941–949. PMLR, 2018.

[6] Jie Chen, Tengfei Ma, and Cao Xiao. Fastgcn: fast learning with graph convolutional networks via importance sampling. *arXiv preprint arXiv:1801.10247*, 2018.

[7] Wei-Lin Chiang, Xuanqing Liu, Si Si, Yang Li, Samy Bengio, and Cho-Jui Hsieh. Cluster-gcn: An efficient algorithm for training deep and large graph convolutional networks. In *Proceedings of the 25th ACM SIGKDD international conference on knowledge discovery & data mining*, pages 257–266, 2019.

[8] Kenneth L Clarkson and David P Woodruff. Low-rank approximation and regression in input sparsity time. *Journal of the ACM (JACM)*, 63(6):1–45, 2017.

[9] Michael B Cohen, Yin Tat Lee, and Zhao Song. Solving linear programs in the current matrix multiplication time. *Journal of the ACM (JACM)*, 68(1):1–39, 2021.

[10] Michael B Cohen, Cameron Musco, and Christopher Musco. Input sparsity time low-rank approximation via ridge leverage score sampling. In *Proceedings of the Twenty-Eighth Annual ACM-SIAM Symposium on Discrete Algorithms*, pages 1758–1777. SIAM, 2017.

[11] Michael B Cohen, Cameron Musco, and Christopher Musco. Input sparsity time low-rank approximation via ridge leverage score sampling. In *Proceedings of the Twenty-Eighth Annual ACM-SIAM Symposium on Discrete Algorithms*, pages 1758–1777. SIAM, 2017.

[12] Sanjoy Dasgupta and Anupam Gupta. An elementary proof of a theorem of johnson and lindenstrauss. *Random Structures & Algorithms*, 22(1):60–65, 2003.

[13] Michał Dereziński and Jiaming Yang. Solving dense linear systems faster than via preconditioning. *arXiv preprint arXiv:2312.08893*, 2023.

[14] Mucong Ding, Kezhi Kong, Jingling Li, Chen Zhu, John Dickerson, Furong Huang, and Tom Goldstein. VQ-GNN: A universal framework to scale up graph neural networks using vector quantization. In Marc'Aurelio Ranzato, Alina Beygelzimer, Yann N. Dauphin, Percy Liang, and Jennifer Wortman Vaughan, editors, *Advances in Neural Information Processing Systems 34: Annual Conference on Neural Information Processing Systems 2021, NeurIPS 2021, December 6-14, 2021, virtual*, pages 6733–6746, 2021.

[15] Petros Drineas and Michael W Mahoney. Randnla: randomized numerical linear algebra. *Communications of the ACM*, 59(6):80–90, 2016.

[16] Matthias Fey, Jan Eric Lenssen, Frank Weichert, and Jure Leskovec. Gnnautoscale: Scalable and expressive graph neural networks via historical embeddings. In Marina Meila and Tong Zhang, editors, *Proceedings of the 38th International Conference on Machine Learning, ICML 2021, 18-24 July 2021, Virtual Event*, volume 139 of *Proceedings of Machine Learning Research*, pages 3294–3304. PMLR, 2021.

[17] Nathan Halko, Per-Gunnar Martinsson, and Joel A Tropp. Finding structure with randomness: Probabilistic algorithms for constructing approximate matrix decompositions. *SIAM review*, 53(2):217–288, 2011.

[18] William L. Hamilton, Zhitao Ying, and Jure Leskovec. Inductive representation learning on large graphs. In Isabelle Guyon, Ulrike von Luxburg, Samy Bengio, Hanna M. Wallach, Rob Fergus, S. V. N. Vishwanathan, and Roman Garnett, editors, *Advances in Neural Information Processing Systems 30: Annual Conference on Neural Information Processing Systems 2017, December 4-9, 2017, Long Beach, CA, USA*, pages 1024–1034, 2017.

[19] Weihua Hu, Matthias Fey, Marinka Zitnik, Yuxiao Dong, Hongyu Ren, Bowen Liu, Michele Catasta, and Jure Leskovec. Open graph benchmark: Datasets for machine learning on graphs. *Advances in neural information processing systems*, 33:22118–22133, 2020.

[20] Haitian Jiang, Renjie Liu, Xiao Yan, Zhenkun Cai, Minjie Wang, and David Wipf. Musegnn: Interpretable and convergent graph neural network layers at scale. *arXiv preprint arXiv:2310.12457*, 2023.

[21] Jonathan A Kelner, Lorenzo Orecchia, Aaron Sidford, and Zeyuan Allen Zhu. A simple, combinatorial algorithm for solving sdd systems in nearly-linear time. In *Proceedings of the forty-fifth annual ACM symposium on Theory of computing*, pages 911–920, 2013.

[22] Thomas N. Kipf and Max Welling. Semi-supervised classification with graph convolutional networks. *CoRR*, abs/1609.02907, 2016.

[23] Ioannis Koutis, Alex Levin, and Richard Peng. Faster spectral sparsification and numerical algorithms for SDD matrices. *ACM Trans. Algorithms*, 12(2):17:1–17:16, 2016.

[24] Meng Liu, Hongyang Gao, and Shuiwang Ji. Towards deeper graph neural networks. In *Proceedings of the 26th ACM SIGKDD international conference on knowledge discovery & data mining*, pages 338–348, 2020.

[25] Xiaorui Liu, Wei Jin, Yao Ma, Yaxin Li, Hua Liu, Yiqi Wang, Ming Yan, and Jiliang Tang. Elastic graph neural networks. In *International Conference on Machine Learning*, pages 6837–6849. PMLR, 2021.

[26] Yao Ma, Xiaorui Liu, Tong Zhao, Yozen Liu, Jiliang Tang, and Neil Shah. A unified view on graph neural networks as graph signal denoising. In *Proceedings of the 30th ACM International Conference on Information & Knowledge Management*, pages 1202–1211, 2021.

[27] Per-Gunnar Martinsson and Joel A Tropp. Randomized numerical linear algebra: Foundations and algorithms. *Acta Numerica*, 29:403–572, 2020.

[28] Xiangrui Meng, Michael A Saunders, and Michael W Mahoney. Lsrn: A parallel iterative solver for strongly over-or underdetermined systems. *SIAM Journal on Scientific Computing*, 36(2):C95–C118, 2014.

[29] Riley Murray, James Demmel, Michael W Mahoney, N Benjamin Erichson, Maksim Melnichenko, Osman Asif Malik, Laura Grigori, Piotr Luszczek, Michał Dereziński, Miles E Lopes, et al. Randomized numerical linear algebra: A perspective on the field with an eye to software. *arXiv preprint arXiv:2302.11474*, 2023.

[30] Kenta Oono and Taiji Suzuki. Graph neural networks exponentially lose expressive power for node classification. *arXiv preprint arXiv:1905.10947*, 2019.

[31] Richard Peng and Daniel A. Spielman. An efficient parallel solver for SDD linear systems. In David B. Shmoys, editor, *Symposium on Theory of Computing, STOC 2014, New York, NY, USA, May 31 - June 03, 2014*, pages 333–342. ACM, 2014.

[32] Richard Peng and Santosh Vempala. Solving sparse linear systems faster than matrix multiplication. In *Proceedings of the 2021 ACM-SIAM symposium on discrete algorithms (SODA)*, pages 504–521. SIAM, 2021.

[33] Vladimir Rokhlin and Mark Tygert. A fast randomized algorithm for overdetermined linear least-squares regression. *Proceedings of the National Academy of Sciences*, 105(36):13212–13217, 2008.

[34] Prithviraj Sen, Galileo Namata, Mustafa Bilgic, Lise Getoor, Brian Galligher, and Tina Eliassi-Rad. Collective classification in network data. *AI magazine*, 29(3):93–93, 2008.

[35] Daniel A Spielman and Nikhil Srivastava. Graph sparsification by effective resistances. In *Proceedings of the fortieth annual ACM symposium on Theory of computing*, pages 563–568, 2008.

[36] Daniel A Spielman and Shang-Hua Teng. Spectral sparsification of graphs. *SIAM Journal on Computing*, 40(4):981–1025, 2011.

[37] Joel A Tropp. Improved analysis of the subsampled randomized hadamard transform. *Advances in Adaptive Data Analysis*, 3(01n02):115–126, 2011.

[38] Nisheeth K Vishnoi et al. Lx = b laplacian solvers and their algorithmic applications. *Foundations and Trends® in Theoretical Computer Science*, 8(1–2):1–141, 2013.

[39] Nisheeth K Vishnoi et al. Lx= b. *Foundations and Trends® in Theoretical Computer Science*, 8(1–2):1–141, 2013.

[40] Minjie Wang, Da Zheng, Zihao Ye, Quan Gan, Mufei Li, Xiang Song, Jinjing Zhou, Chao Ma, Lingfan Yu, Yu Gai, Tianjun Xiao, Tong He, George Karypis, Jinyang Li, and Zheng Zhang. Deep graph library: A graph-centric, highly-performant package for graph neural networks. *arXiv preprint arXiv:1909.01315*, 2019.

[41] David P Woodruff et al. Sketching as a tool for numerical linear algebra. *Foundations and Trends® in Theoretical Computer Science*, 10(1–2):1–157, 2014.

[42] Keyulu Xu, Weihua Hu, Jure Leskovec, and Stefanie Jegelka. How powerful are graph neural networks? *arXiv preprint arXiv:1810.00826*, 2018.

[43] Rui Xue, Haoyu Han, MohamadAli Torkamani, Jian Pei, and Xiaorui Liu. Lazygnn: Large-scale graph neural networks via lazy propagation. *arXiv preprint arXiv:2302.01503*, 2023.

[44] Chaoqi Yang, Ruijie Wang, Shuochao Yao, Shengzhong Liu, and Tarek Abdelzaher. Revisiting over-smoothing in deep gcns. *arXiv preprint arXiv:2003.13663*, 2020.

[45] Yongyi Yang, Tang Liu, Yangkun Wang, Zengfeng Huang, and David Wipf. Implicit vs unfolded graph neural networks. *arXiv preprint arXiv:2111.06592*, 2021.

[46] Yongyi Yang, Tang Liu, Yangkun Wang, Jinjing Zhou, Quan Gan, Zhewei Wei, Zheng Zhang, Zengfeng Huang, and David Wipf. Graph neural networks inspired by classical iterative algorithms. In Marina Meila and Tong Zhang, editors, *Proceedings of the 38th International Conference on Machine Learning, ICML 2021, 18-24 July 2021, Virtual Event*, volume 139 of *Proceedings of Machine Learning Research*, pages 11773–11783. PMLR, 2021.

[47] Hanqing Zeng, Muhan Zhang, Yinglong Xia, Ajitesh Srivastava, Andrey Malevich, Rajgopal Kannan, Viktor Prasanna, Long Jin, and Ren Chen. Decoupling the depth and scope of graph neural networks. *Advances in Neural Information Processing Systems*, 34:19665–19679, 2021.

[48] Hongwei Zhang, Tijin Yan, Zenjun Xie, Yuanqing Xia, and Yuan Zhang. Revisiting graph convolutional network on semi-supervised node classification from an optimization perspective. *arXiv preprint arXiv:2009.11469*, 2020.

[49] Jiong Zhu, Yujun Yan, Lingxiao Zhao, Mark Heimann, Leman Akoglu, and Danai Koutra. Beyond homophily in graph neural networks: Current limitations and effective designs. *Advances in neural information processing systems*, 33:7793–7804, 2020.

[50] Meiqi Zhu, Xiao Wang, Chuan Shi, Houye Ji, and Peng Cui. Interpreting and unifying graph neural networks with an optimization framework. In *Proceedings of the Web Conference 2021*, pages 1215–1226, 2021.

[51] Daniel Zügner, Amir Akbarnejad, and Stephan Günnemann. Adversarial attacks on neural networks for graph data. In *Proceedings of the 24th ACM SIGKDD international conference on knowledge discovery & data mining*, pages 2847–2856, 2018.

A Introduction to the Mathematical Tools

In the main paper, due to space limitations, our introduction of certain mathematical tools and concepts remains brief. In this section, we provide a more comprehensive introduction to the mathematical tools utilized in the main paper.

A.1 Subsampling

Subsampling is used in multiple places in our Algorithm. When we say subsampling s rows of a matrix $\boldsymbol{M} \in \mathbb{R}^{n\times d}$ with probability $\{p_k\}_{k=1}^n$ and obtain a new matrix $\tilde{\boldsymbol{M}} \in \mathbb{R}^{s\times d}$, it means each row of $\tilde{\boldsymbol{M}}$ is an i.i.d. random vector which follows the same distribution of a random vector $\boldsymbol{\xi}$ that satisfies the following property:

$$\mathbb{P}\left\{\boldsymbol{\xi} = \sqrt{\frac{1}{sp_k}}\boldsymbol{m}_k\right\} = p_k, \tag{A.1}$$

where $\boldsymbol{m}_k$ is the k-th row of matrix $\boldsymbol{M}$. It is clear that constructing such a subsampled matrix $\tilde{\boldsymbol{M}}$ takes time $O(sd)$. Moreover, if $p_k = \frac{1}{n}$, we say the subsampling is with uniform probability.

The operator of subsampling s rows of a n-row matrix is clearly a linear transformation. Therefore it can be represented by a random matrix $\boldsymbol{S} \in \mathbb{R}^{s\times n}$. Notice that when we apply $\boldsymbol{S}$ to a matrix (i.e. $\boldsymbol{S}\cdot\boldsymbol{M}$) we don't actually need to construct such a matrix $\boldsymbol{S}$ and calculate matrix product, since we only carry out sampling.

A.2 SDD Solvers

As mentioned in the main paper, for a sparse SDD matrix $\boldsymbol{M}$, it is possible to fast approximate its linear solver. The following Lemma A.1 rigorously states the bound we can obtain for SDD solvers.

Lemma A.1 ([31]). *For any SDD matrix $\boldsymbol{M} \in \mathbb{R}^{n\times n}$ and any real number $\epsilon > 0$, there exists an algorithm to construct an operator $\mathsf{SSolve}_\epsilon(\boldsymbol{M};\cdot)$, such that $\mathsf{SSolve}_\epsilon(\boldsymbol{M};\cdot)$ is a linear solver for $\boldsymbol{M}$ with ϵ error rate and for any $\boldsymbol{x} \in \mathbb{R}^n$, calculating $\mathsf{SSolve}_\epsilon(\boldsymbol{M};\boldsymbol{x})$ takes time*

$$O\left(m\left(\log\frac{1}{\epsilon}\right)\operatorname{poly}\log(m)\operatorname{poly}\log\left(\kappa(\boldsymbol{M})\right)\right), \tag{A.2}$$

where $m = \operatorname{nnz}(\boldsymbol{M})$.

A.3 Fast Matrix Multiplication

As mentioned in the main paper, we use SRHT to achieve fast matrix multiplication. Here we further explain this process. We refer interested readers to [37] for more details. For a positive integer number n that is a power of 2, the Hadamard transformation of size n is a linear transformation recursively defined as follows:

$$\boldsymbol{H}_n := \begin{bmatrix}\boldsymbol{H}_{n/2} & \boldsymbol{H}_{n/2}\\ \boldsymbol{H}_{n/2} & -\boldsymbol{H}_{n/2}\end{bmatrix} \tag{A.3}$$

and $\boldsymbol{H}_1 = 1$. For a vector $\boldsymbol{x} \in \mathbb{R}^n$, we define

$$\mathsf{Hadamard}(\boldsymbol{x}) := \frac{1}{\sqrt{n}}\boldsymbol{H}_n\boldsymbol{x}. \tag{A.4}$$

Notice that when n is not a power of 2, we pad the vector $\boldsymbol{x}$ with 0-s beforehand, therefore the requirement of n being a power of 2 is ignored in the actual usage. From its recursive nature, it is not hard to see that applying a Hadamard transformation to each column of an $n \times d$ matrix only takes $O(d\log n)$ time.

Let $\boldsymbol{R} \in \mathbb{R}^{n\times n}$ be a diagonal matrix whose diagonal entries are i.i.d. Rademacher variables, and $\boldsymbol{S} \in \mathbb{R}^{s\times n}$ be a subsampling matrix with uniform probability and $s = O\left(\frac{d}{\beta^2}\log n\right)$. For a matrix $\boldsymbol{Q} \in \mathbb{R}^{n\times d}$, its SRHT with β error rate is defined as

$$\mathsf{SRHT}_\beta(\boldsymbol{Q}) := \boldsymbol{S}\mathsf{Hadamard}\left(\boldsymbol{R}\boldsymbol{Q}\right), \tag{A.5}$$

which is exactly the matrix $\tilde{\boldsymbol{Q}}$ we use in Algorithm 1. A fast matrix multiplication result can be achieved using SRHT.

Lemma A.2 ([37]). *For matrix $\boldsymbol{Q} \in \mathbb{R}^{n\times d}$ where $n \geq d$ and $\mathrm{rank}(\boldsymbol{Q}) = d$, let $\tilde{\boldsymbol{Q}} = \mathsf{SRHT}_\beta(\boldsymbol{Q})$ where $\beta \in (0, 1/4)$, then we have*

$$\tilde{\boldsymbol{Q}}^\top \tilde{\boldsymbol{Q}} \approx_\beta \boldsymbol{Q}^\top \boldsymbol{Q} \tag{A.6}$$

with probability at least $1 - \frac{1}{2n}$.

B Running Time of the Original Implementation Used in [46]

In this section we analyze the time complexity of the implementation used in [46], which uses gradient descent to solve both inner and outer problem.

Inner Problem Analysis. We first analyze the time complexity of the inner problem solver used in [46]. Recall that for the inner problem eq.(4.3), we need to find an approximation of the linear solver of $\boldsymbol{I} + \lambda\hat{\boldsymbol{L}}$. In [46], it is implemented by a standard gradient descent. Here we consider approximately solving the following least square problem by gradient descent:

$$\boldsymbol{v} = \arg\min_{\boldsymbol{v}\in\mathbb{R}^n} \frac{1}{2}\left\|\left(\boldsymbol{I} + \lambda\hat{\boldsymbol{L}}\right)\boldsymbol{v} - \boldsymbol{u}\right\|_2^2. \tag{B.1}$$

The gradient step with step size μ is:

$$\boldsymbol{v}^{(t+1)} = (1-\mu)\left(\boldsymbol{I} + \lambda\hat{\boldsymbol{L}}\right)^2 \boldsymbol{v}^{(t)} + \eta\left(\boldsymbol{I} + \lambda\hat{\boldsymbol{L}}\right)\boldsymbol{u}. \tag{B.2}$$

Theorem B.1 (Inner Analysis). *If we update $\boldsymbol{v}^{(t)}$ through eq.(B.2) with initialization $\boldsymbol{v}^{(0)} = \boldsymbol{0}$ and a proper η, then after $T = O\left(\lambda^2 \log\frac{\lambda}{\epsilon^2}\right)$ iterations we can get*

$$\left\|\boldsymbol{v}^{(T)} - \left(\boldsymbol{I} + \lambda\hat{\boldsymbol{L}}\right)^{-1}\boldsymbol{u}\right\|_{(\boldsymbol{I}+\lambda\hat{\boldsymbol{L}})} \leq \epsilon\left\|\left(\boldsymbol{I} + \lambda\hat{\boldsymbol{L}}\right)^{-1}\boldsymbol{u}\right\|_{(\boldsymbol{I}+\lambda\hat{\boldsymbol{L}})} \tag{B.3}$$

for any $\epsilon \in (0, 1)$.

Proof. Let $\boldsymbol{H} = \boldsymbol{I} + \lambda\hat{\boldsymbol{L}}$. Notice that the strongly convexity and Lipschitz constant of Problem eq.(B.1) is $\mathscr{C} = 1$ and $L \leq 9\lambda^2$ respectively. From Lemma C.1, take $\eta = \frac{1}{L}$ and $\boldsymbol{v}^{(0)} = \boldsymbol{0}$, we have

$$\|\boldsymbol{H}\boldsymbol{v}^{(T)} - \boldsymbol{u}\|^2 \leq (1 - 9\lambda^2)^T\|\boldsymbol{u}\|^2 \tag{B.4}$$

for any $T \in \mathbb{N}$. Therefore,

$$\frac{\|\boldsymbol{v}^{(T)} - \boldsymbol{H}^{-1}\boldsymbol{u}\|_{\boldsymbol{H}}^2}{\|\boldsymbol{H}^{-1}\boldsymbol{u}\|_{\boldsymbol{H}}^2} = \frac{\|\boldsymbol{H}\boldsymbol{v}^{(T)} - \boldsymbol{u}\|_{\boldsymbol{H}^{-1}}^2}{\|\boldsymbol{u}\|_{\boldsymbol{H}^{-1}}^2} \tag{B.5}$$

$$\leq 3\lambda\frac{\|\boldsymbol{H}\boldsymbol{v}^{(T)} - \boldsymbol{u}\|_2^2}{\|\boldsymbol{u}\|_2^2} \tag{B.6}$$

$$\leq 3\lambda(1 - 9\lambda^2)^T. \tag{B.7}$$

To obtain an error rate ϵ, the smallest number of iterations T needed is

$$T = \left(\log\frac{1}{1-(9\lambda^2)^{-1}}\right)^{-1}\log\frac{3\lambda}{\epsilon^2} + 1 = O\left[\left(\log\frac{1}{1-\lambda^{-2}}\right)^{-1}\log\frac{\kappa}{\epsilon^2}\right] = O\left(\lambda^2\log\frac{\lambda}{\epsilon^2}\right). \tag{B.8}$$

□

Overall Running Time. As we proved above in Theorem B.1, the number of iterations needed for solving the inner problem to error rate β with the implementation of [46] is $\tilde{O}\left(\lambda^2\log\frac{1}{\beta}\right)$, which is related to the hyper-parameter λ. For each inner iteration (i.e. eq.(B.2)), we need to compute $(\boldsymbol{I} + \lambda\boldsymbol{L})(\boldsymbol{X}\boldsymbol{w} - \hat{\boldsymbol{y}})$. Since this is a sparse matrix multiplication, the complexity of this step is $O(m + nd)$. Putting things together, we have the time complexity of calling inner problem solver is $\tilde{O}\left((m + nd)\lambda^2\log\frac{1}{\beta}\right)$.

From Lemma 5.1, the number of outer iterations needed is $\tilde{O}\left(\kappa_o \log \frac{1}{\epsilon}\right)$, where κ_o is the condition number of the outer problem. Moreover, Lemma 5.1 also indicates that we require $\beta \leq \frac{\epsilon^{1/2}}{25\kappa(\boldsymbol{X})\lambda}$, so solving inner problem takes $\tilde{O}(\lambda^2 \log 1/\beta) = \tilde{O}(\lambda^2 \log 1/\epsilon)$. In each outer iteration, we need to call inner problem solver constant times, and as well as performing constant matrix vector multiplications whose complexity is $O(nd)$. Therefore the overall running time of solving the training problem is $\tilde{O}\left[\kappa_o \left(\lambda^2(m+nd)+nd\right)\left(\log \frac{1}{\epsilon}\right)^2\right]$.

C Proof of Theoretical Results

We first note that since $\hat{\boldsymbol{L}}$ is normalized, all the eigenvalues of $\hat{\boldsymbol{L}}$ are in the range $[0, 2)$. Therefore, we have $\sigma_{\min}(\boldsymbol{I} + \lambda\hat{\boldsymbol{L}}) = 1$ and $\sigma_{\max}(\boldsymbol{I} + \lambda\hat{\boldsymbol{L}}) \leq 1 + 2\lambda$. In the whole paper we view λ as a large value (i.e. $\lambda \gg 1$). In practice, it is possible to use a small λ, in which case the algorithm works no worse than the case where $\lambda = 1$. Therefore the λ used in the paper should actually be understood as $\max\{\lambda, 1\}$. With this assumption, below we assume $\sigma_{\max}(\boldsymbol{I} + \lambda\hat{\boldsymbol{L}}) \leq 3\lambda$ for convenience.

C.1 Descent Lemma

In this subsection, we introduce a descent lemma that we will use to analyze the convergence rate. This is a standard result in convex optimization, and we refer interested readers to [3] for more details.

Lemma C.1. *If $\ell : \mathbb{R}^d \to \mathbb{R}$ is L-Lipschitz smooth and c-strongly convex, and we have a sequence of points $\left\{\boldsymbol{w}^{(t)}\right\}_{t=1}^{T}$ in $\mathbb{R}^d$ such that*

$$\boldsymbol{w}^{(t+1)} = \boldsymbol{w}^{(t)} - \eta \boldsymbol{g}^{(t)}, \tag{C.1}$$

where $\left\|\boldsymbol{g}^{(t)} - \nabla\ell\left(\boldsymbol{w}^{(t)}\right)\right\|_2 \leq \gamma \left\|\nabla\ell\left(\boldsymbol{w}^{(t)}\right)\right\|_2$ and $\gamma < 1$, $\eta = \frac{1-\gamma}{(1+\gamma)^2 L}$, then we have

$$\ell\left(\boldsymbol{w}^{(T)}\right) - \ell^* \leq \left[1 - \kappa^{-1}\left(\frac{1-\gamma}{1+\gamma}\right)^2\right]^T \left[\ell\left(\boldsymbol{w}^{(0)}\right) - \ell^*\right], \tag{C.2}$$

where $\ell^* = \inf_{\boldsymbol{w}\in\mathbb{R}^d} \ell(\boldsymbol{w})$ and $\kappa = \frac{L}{c}$.

Proof. From the condition $\left\|\boldsymbol{g}^{(t)} - \nabla\ell\left(\boldsymbol{w}^{(t)}\right)\right\|_2 \leq \gamma \left\|\nabla\ell\left(\boldsymbol{w}^{(t)}\right)\right\|_2$, we have that

$$(1-\gamma)\|\boldsymbol{g}^{(t)}\|_2 \leq \left\|\nabla\ell\left(\boldsymbol{w}^{(t)}\right)\right\|_2 \leq (1+\gamma)\|\boldsymbol{g}^{(t)}\|_2 \tag{C.3}$$

and

$$-2\left\langle g^{(t)}, \nabla\ell\left(\boldsymbol{w}^{(t)}\right)\right\rangle = \left\|\boldsymbol{g}^{(t)} - \nabla\ell\left(\boldsymbol{w}^{(t)}\right)\right\|_2^2 - \left\|\boldsymbol{g}^{(t)}\right\|_2^2 - \left\|\nabla\ell\left(\boldsymbol{w}^{(t)}\right)\right\|_2^2 \tag{C.4}$$

$$\leq \left[(\gamma^2 - 1) - (1-\gamma)^2\right]\left\|\nabla\ell\left(\boldsymbol{w}^{(t)}\right)\right\|_2^2 \tag{C.5}$$

$$= 2(\gamma - 1)\left\|\nabla\ell\left(\boldsymbol{w}^{(t)}\right)\right\|_2^2 \tag{C.6}$$

From Lipschitz smoothness, we have

$$\ell\left(\boldsymbol{w}^{(t+1)}\right) - \ell\left(\boldsymbol{w}^{(t)}\right) \leq -\eta\left\langle \boldsymbol{g}^{(t)}, \nabla\ell\left(\boldsymbol{w}^{(t)}\right)\right\rangle + \frac{1}{2}L\eta^2\|\boldsymbol{g}^{(t)}\|_2^2 \tag{C.7}$$

$$\leq \left(\eta(\gamma-1) + \frac{1}{2}L\eta^2(1+\gamma)^2\right)\left\|\nabla\ell\left(\boldsymbol{w}^{(t)}\right)\right\|_2^2. \tag{C.8}$$

It's not hard to show that the optimal η for eq.(C.8) is $\eta = \frac{1-\gamma}{L(1+\gamma)^2}$. Substituting $\eta = \frac{1-\gamma}{L(1+\gamma)^2}$ to eq.(C.8) and use convexity we can get

$$\ell\left(\boldsymbol{w}^{(t+1)}\right) - \ell^* \leq \left[\ell\left(\boldsymbol{w}^{(t)}\right) - \ell^*\right] - \frac{(1-\gamma)^2}{2L(1+\gamma)^2}\left\|\nabla\ell\left(\boldsymbol{w}^{(t)}\right)\right\|_2^2 \tag{C.9}$$

$$\leq \left[\ell\left(\boldsymbol{w}^{(t)}\right) - \ell^*\right] - \frac{c(1-\gamma)^2}{L(1+\gamma)^2}\left[\ell\left(\boldsymbol{w}^{(t)}\right) - \ell^*\right] \tag{C.10}$$

By induction we have

$$\ell\left(\boldsymbol{w}^{(T)}\right)-\ell^{*}\leq\left[1-\kappa^{-1}\left(\frac{1-\gamma}{1+\gamma}\right)^{2}\right]^{T}\left[\ell\left(\boldsymbol{w}^{(0)}\right)-\ell^{*}\right]. \tag{C.11}$$

□

C.2 Bound of Loss Value by Gradient

In this subsection, we derive an inequality that allows us to bound the value of loss function by the norm of gradient.

Lemma C.2. *If $\ell:\mathbb{R}^{d}\to\mathbb{R}$ is a $\mathscr{C}$-strongly convex and smooth function, and $\boldsymbol{w}^{*}=\arg\min_{\boldsymbol{w}\in\mathbb{R}^{d}}\ell(\boldsymbol{w})$ is a global optimal, then for any $\boldsymbol{w}\in\mathbb{R}^{d}$ and $\epsilon\in(0,1)$, we have*

$$\ell(\boldsymbol{w})\leq\max\left\{(1+\epsilon)\ell(\boldsymbol{w}^{*}),\frac{1}{\epsilon\mathscr{C}}\|\nabla\ell(\boldsymbol{w})\|^{2}\right\}. \tag{C.12}$$

Proof. Using the inequality (4.12) from [3], we have

$$\ell(\boldsymbol{w})\leq\frac{1}{2\mathscr{C}}\|\nabla\ell(\boldsymbol{w})\|^{2}+\ell(\boldsymbol{w}^{*}). \tag{C.13}$$

If $\ell(\boldsymbol{w})\geq(1+\epsilon)\ell(\boldsymbol{w}^{*})$, we have

$$\ell(\boldsymbol{w})\leq\frac{1}{2\mathscr{C}}\|\nabla\ell(\boldsymbol{w})\|^{2}+\frac{1}{1+\epsilon}\ell(\boldsymbol{w}). \tag{C.14}$$

Shifting the terms in eq.(C.14) gives $\ell(\boldsymbol{w})\leq\frac{1+\epsilon}{2\mathscr{C}\epsilon}\|\nabla\ell(\boldsymbol{w})\|^{2}\leq\frac{1}{\epsilon\mathscr{C}}\|\nabla\ell(\boldsymbol{w})\|^{2}$, which proves the claim.

□

C.3 Proof of Lemma 5.1

Given a point $\boldsymbol{w}\in\mathbb{R}^{d}$, we first consider the error between the estimated gradient $\widetilde{\nabla\ell_{i}(\boldsymbol{w})}$ and the true gradient $\nabla\ell_{i}(\boldsymbol{w})$. Below we denote $\boldsymbol{H}=\boldsymbol{I}+\lambda\hat{\boldsymbol{L}}$ and $\boldsymbol{z}=\boldsymbol{X}\boldsymbol{w}-\hat{\boldsymbol{y}}_{i}$. It's not hard to notice that $\ell_{i}(\boldsymbol{w})=\frac{1}{2}\left\|\boldsymbol{H}^{-1}\boldsymbol{z}\right\|^{2}$ and $\nabla\ell_{i}(\boldsymbol{w})=\boldsymbol{X}^{\top}\boldsymbol{H}^{-2}\boldsymbol{z}$. Moreover, we denote $\ell_{i}^{*}=\inf_{\boldsymbol{w}}\ell_{i}^{*}$ as the optimal value of ℓ_{i}.

we have

$$\begin{aligned}\left\|\widetilde{\nabla\ell_{i}(\boldsymbol{w})}-\nabla\ell_{i}(\boldsymbol{w})\right\| &= \left\|\boldsymbol{X}^{\top}\left[\mathcal{S}\left(\boldsymbol{H}^{-1}\boldsymbol{z}\right)-\boldsymbol{H}^{-2}\boldsymbol{z}+\mathcal{S}(\mathcal{S}(\boldsymbol{z}))-\mathcal{S}\left(\boldsymbol{H}^{-1}\boldsymbol{z}\right)\right]\right\| &\text{(C.15)}\\ &\leq \left\|\boldsymbol{X}^{\top}\left[\mathcal{S}\left(\boldsymbol{H}^{-1}\boldsymbol{z}\right)-\boldsymbol{H}^{-2}\boldsymbol{z}\right]\right\|+\left\|\boldsymbol{X}^{\top}\left[\mathcal{S}(\mathcal{S}(\boldsymbol{z})-\boldsymbol{H}^{-1}\boldsymbol{z})\right]\right\|. &\text{(C.16)}\end{aligned}$$

As shown, the gradient error can be decomposed into two terms, namely $\left\|\widetilde{\nabla\ell_{i}(\boldsymbol{w})}-\nabla\ell_{i}(\boldsymbol{w})\right\|=E_{1}+E_{2}$, where $E_{1}=\left\|\boldsymbol{X}^{\top}\left[\mathcal{S}\left(\boldsymbol{H}^{-1}\boldsymbol{z}\right)-\boldsymbol{H}^{-2}\boldsymbol{z}\right]\right\|$ and $E_{2}=\left\|\boldsymbol{X}^{\top}\left[\mathcal{S}(\mathcal{S}(\boldsymbol{z})-\boldsymbol{H}^{-1}\boldsymbol{z})\right]\right\|$. Below we analyze each part separately.

Notice that, as we assumed $\boldsymbol{X}$ is full-rank, ℓ_{i} is a strongly convex function with parameter $\mathscr{C}=\sigma_{\min}\left(\boldsymbol{X}^{\top}\boldsymbol{H}^{-2}\boldsymbol{X}\right)\geq\frac{\sigma_{\min}(\boldsymbol{X})^{2}}{9\lambda^{2}}$. Let $\mathcal{D}=\left\{\boldsymbol{w}\in\mathbb{R}^{d}\middle|\,\ell_{i}(\boldsymbol{w})\leq(1+\epsilon)\ell_{i}^{*}\right\}$. If $\boldsymbol{w}\in\mathcal{D}$, then $\boldsymbol{w}$ is already a good enough solution. Below we assume $\boldsymbol{w}\notin\mathcal{D}$, in which case by Lemma C.2, we have $\ell_{i}(\boldsymbol{w})\leq\frac{1}{\epsilon\mathscr{C}}\|\nabla\ell_{i}(\boldsymbol{w})\|^{2}$, which means

$$\left\|\boldsymbol{H}^{-1}\boldsymbol{z}\right\|^{2}\leq\frac{2}{\mathscr{C}\epsilon}\left\|\boldsymbol{X}^{-1}\boldsymbol{H}^{-2}\boldsymbol{z}\right\|^{2}\leq\frac{18\lambda^{2}}{\sigma_{\min}(\boldsymbol{X})^{2}\epsilon}. \tag{C.17}$$

For E_1, we have

$$E_1 = \left\|\boldsymbol{X}^\top \left[\mathcal{S}\left(\boldsymbol{H}^{-1}\boldsymbol{z}\right) - \boldsymbol{H}^{-2}\boldsymbol{z}\right]\right\|_2 \tag{C.18}$$
$$\leq \sigma_{\max}(\boldsymbol{X}) \left\|\mathcal{S}\left(\boldsymbol{H}^{-1}\boldsymbol{z}\right) - \boldsymbol{H}^{-2}\boldsymbol{z}\right\|_2 \tag{C.19}$$
$$\leq \sigma_{\max}(\boldsymbol{X}) \left\|\mathcal{S}\left(\boldsymbol{H}^{-1}\boldsymbol{z}\right) - \boldsymbol{H}^{-2}\boldsymbol{z}\right\|_{\boldsymbol{H}} \tag{C.20}$$
$$\leq \sigma_{\max}(\boldsymbol{X})\mu \left\|\boldsymbol{H}^{-2}\boldsymbol{z}\right\|_{\boldsymbol{H}} \tag{C.21}$$
$$\leq \sigma_{\max}(\boldsymbol{X})\mu \left\|\boldsymbol{H}^{-1}\boldsymbol{z}\right\|_2 \tag{C.22}$$
$$\leq \sqrt{\frac{18}{\epsilon}}\kappa(\boldsymbol{X})\lambda\mu \left\|\boldsymbol{X}^\top\boldsymbol{H}^{-2}\boldsymbol{z}\right\|_2 \tag{C.23}$$
$$\leq 5\epsilon^{-1/2}\kappa(\boldsymbol{X})\lambda\mu\|\nabla\ell_i(\boldsymbol{w})\|_2. \tag{C.24}$$

For E_2, we have

$$E_2 = \left\|\boldsymbol{X}^\top \left[\mathcal{S}(\mathcal{S}(\boldsymbol{z}) - \boldsymbol{H}^{-1}\boldsymbol{z})\right]\right\|_2 \tag{C.25}$$
$$\leq \sigma_{\max}(\boldsymbol{X})(1+\mu)\|\boldsymbol{H}^{-1}\left(\mathcal{S}(\boldsymbol{z}) - \boldsymbol{H}^{-1}\boldsymbol{z}\right)\|_{\boldsymbol{H}} \tag{C.26}$$
$$\leq \sigma_{\max}(\boldsymbol{X})(1+\mu)\|\mathcal{S}(\boldsymbol{z}) - \boldsymbol{H}^{-1}\boldsymbol{z}\|_{\boldsymbol{H}} \tag{C.27}$$
$$\leq \sigma_{\max}(\boldsymbol{X})(1+\mu)\mu\|\boldsymbol{H}^{-1}\boldsymbol{z}\|_{\boldsymbol{H}} \tag{C.28}$$
$$\leq \sqrt{\frac{18}{\epsilon}}\kappa(\boldsymbol{X})(1+\mu)\mu\lambda\sqrt{3\lambda}\|\boldsymbol{X}^\top\boldsymbol{H}^{-2}\boldsymbol{z}\|_2 \tag{C.29}$$
$$\leq 20\epsilon^{-1/2}\kappa(\boldsymbol{X})\mu\lambda^2\|\nabla\ell_i(\boldsymbol{w}_i)\|_2. \tag{C.30}$$

Combine the bound of E_1 and E_2, we have

$$\left\|\widetilde{\nabla\ell_i(\boldsymbol{w}_i)} - \nabla\ell_i(\boldsymbol{w}_i)\right\| \leq E_1 + E_2 \leq 25\epsilon^{-1/2}\kappa(\boldsymbol{X})\mu\lambda^2\|\nabla\ell_i(\boldsymbol{w}_i)\|_2. \tag{C.31}$$

Now, consider the optimization. Let $\left\{\boldsymbol{w}_i^{(t)}\right\}_{t=1}^T$ be a sequence such that

$$\boldsymbol{w}_i^{(t+1)} = \boldsymbol{w}^{(t)} - \eta\widetilde{\nabla\ell_i\left(\boldsymbol{w}_i^{(t)}\right)}. \tag{C.32}$$

Let κ be the condition number of $\boldsymbol{X}^\top\boldsymbol{H}^{-2}\boldsymbol{X}$ and let ℓ_i^* be the optimal value of ℓ_i. Let $\gamma = 25\epsilon^{-1/2}\kappa(\boldsymbol{X})\lambda^2\mu \leq \frac{1}{2}$. From Lemma C.1, we have with a proper value of η,

$$\ell_i\left(\boldsymbol{w}_i^{(T)}\right) - \ell^* \leq \left(1 - \left(\frac{1-\gamma}{1+\gamma}\right)^2\kappa^{-1}\right)^T \left[\ell_i\left(\boldsymbol{w}_i^{(0)}\right) - \ell_i^*\right] \tag{C.33}$$
$$\leq \left(1 - (9\kappa)^{-1}\right)^T \left[\ell_i\left(\boldsymbol{w}_i^{(0)}\right) - \ell_i^*\right]. \tag{C.34}$$

Therefore, the number of iterations T required to achieve ϵ error rate is

$$T = O\left(\left(\log\frac{1}{1-(9\kappa)^{-1}}\right)^{-1}\log\frac{1}{\epsilon}\right) = O\left(\kappa\log\frac{1}{\epsilon}\right). \tag{C.35}$$

C.4 Proof of Lemma 5.2

The basic idea of Algorithm 2 is to use ridge leverage score sampling methods to obtain a spectral sparsifier. Let $\hat{\boldsymbol{B}} = \boldsymbol{B}\boldsymbol{D}^{-1/2}$ be the normalized incidence matrix and $\hat{\boldsymbol{b}}_i$ the i-th row of $\hat{\boldsymbol{B}}$. Given $\lambda^{-1} > 0$, for $i \in \{1, 2, \cdots, m\}$, the i-th ridge leverage score is defined as

$$l_i := \hat{\boldsymbol{b}}_i^\top(\hat{\boldsymbol{L}} + \lambda^{-1}\boldsymbol{I})^{-1}\hat{\boldsymbol{b}}_i \tag{C.36}$$
$$= \hat{\boldsymbol{b}}_i^\top(\hat{\boldsymbol{L}} + \lambda^{-1}\boldsymbol{I})^{-1}\hat{\boldsymbol{L}}(\hat{\boldsymbol{L}} + \lambda^{-1}\boldsymbol{I})^{-1}\hat{\boldsymbol{b}}_i + \lambda^{-1}\hat{\boldsymbol{b}}_i^\top(\hat{\boldsymbol{L}} + \lambda^{-1}\boldsymbol{I})^{-2}\hat{\boldsymbol{b}}_i \tag{C.37}$$
$$= \|\hat{\boldsymbol{B}}(\hat{\boldsymbol{L}} + \lambda^{-1}\boldsymbol{I})^{-1}\hat{\boldsymbol{b}}_i\|^2 + \lambda^{-1}\|(\hat{\boldsymbol{L}} + \lambda^{-1}\boldsymbol{I})^{-1}\hat{\boldsymbol{b}}_i\|^2. \tag{C.38}$$

It is not affordable to compute all the m ridge leverage scores exactly. Therefore, we first use Johnson–Lindenstrauss lemma to reduce the dimension. Recall that in Algorithm 2 we define $\boldsymbol{\Pi}_1 \in \mathbb{R}^{k\times m}$ and $\boldsymbol{\Pi}_2 \in \mathbb{R}^{k\times n}$ to be Gaussian sketches (that is, each entry of the matrices are i.i.d Gaussian random variables $\mathcal{N}(0, 1/k)$). We set $k = O(\log m)$, and by using Lemma C.3 we have the following claim holds with probability at least $1 - \frac{1}{8n}$:

$$\|\boldsymbol{\Pi}_1\hat{\boldsymbol{B}}(\hat{\boldsymbol{L}} + \lambda^{-1}\boldsymbol{I})^{-1}\hat{\boldsymbol{b}}_i\| \approx_{2^{1/4}-1} \|\hat{\boldsymbol{B}}(\hat{\boldsymbol{L}} + \lambda^{-1}\boldsymbol{I})^{-1}\hat{\boldsymbol{b}}_i\| \quad \text{for all } i \in \{1, 2, \cdots, m\}. \tag{C.39}$$

Similarly,the following claim also holds with probability at least $1 - \frac{1}{8n}$:

$$\|\boldsymbol{\Pi}_2(\hat{\boldsymbol{L}} + \lambda^{-1}\boldsymbol{I})^{-1}\hat{\boldsymbol{b}}_i\| \approx_{2^{1/4}-1} \|(\hat{\boldsymbol{L}} + \lambda^{-1}\boldsymbol{I})^{-1}\hat{\boldsymbol{b}}_i\| \quad \text{for all } i \in \{1, 2, \cdots, m\}. \tag{C.40}$$

By summing over above two inequalities (after squared) and taking an union bound, with probability $1 - \frac{1}{4n}$ we have

$$\|\boldsymbol{\Pi}_1\hat{\boldsymbol{B}}(\hat{\boldsymbol{L}} + \lambda^{-1}\boldsymbol{I})^{-1}\hat{\boldsymbol{b}}_i\|^2 + \lambda^{-1}\|\boldsymbol{\Pi}_2(\hat{\boldsymbol{L}} + \lambda^{-1}\boldsymbol{I})^{-1}\hat{\boldsymbol{b}}_i\|^2 \approx_{\sqrt{2}-1} l_i \quad \text{for all} \quad i \in \{1, 2, \cdots, m\}. \tag{C.41}$$

However it is still too expensive to compute $\boldsymbol{\Pi}_1\hat{\boldsymbol{B}}(\hat{\boldsymbol{L}} + \lambda^{-1}\boldsymbol{I})^{-1}$ and $\boldsymbol{\Pi}_2(\hat{\boldsymbol{L}} + \lambda^{-1}\boldsymbol{I})^{-1}$, since computing $(\hat{\boldsymbol{L}} + \lambda^{-1}\boldsymbol{I})^{-1}$ itself takes prohibitive $O(n^3)$ time. Instead, notice that $\hat{\boldsymbol{L}} + \lambda^{-1}\boldsymbol{I}$ is a SDD matrix, thus we can apply the SDD solver to the k columns of matrix $(\boldsymbol{\Pi}_1\hat{\boldsymbol{B}})^\top$ and $(\boldsymbol{\Pi}_2)^\top$ respectively. According to Lemma A.1, there is a linear operator $\mathsf{SSolve}_\epsilon(\hat{\boldsymbol{L}} + \lambda^{-1}\boldsymbol{I}; \boldsymbol{x})$ that runs in time $\tilde{O}(\mathrm{nnz}(\hat{\boldsymbol{L}} + \lambda^{-1}\boldsymbol{I}) \cdot \log 1/\epsilon) = \tilde{O}(m \log 1/\epsilon)$ such that for any $\boldsymbol{x}^\top \in \mathbb{R}^n$, it outputs $\tilde{\boldsymbol{x}}$ that satisfies $\|\tilde{\boldsymbol{x}} - \boldsymbol{x}^\top(\hat{\boldsymbol{L}} + \lambda^{-1}\boldsymbol{I})^{-1}\|_{\hat{\boldsymbol{L}}+\lambda^{-1}\boldsymbol{I}} \le \epsilon\|\boldsymbol{x}^\top(\hat{\boldsymbol{L}} + \lambda^{-1})\|_{\hat{\boldsymbol{L}}+\lambda^{-1}\boldsymbol{I}}$. For our purpose we set $\epsilon = 2^{1/4}$. Denote $\boldsymbol{B}_{\mathcal{S}}$ as the matrix obtained by applying each column of $(\boldsymbol{\Pi}_1\hat{\boldsymbol{B}})^\top$ to $\mathsf{SSolve}_\epsilon(\hat{\boldsymbol{L}} + \lambda^{-1}\boldsymbol{I}; \boldsymbol{x})$, that is, the j-th row of $\mathsf{SSolve}_{2^{1/4}}(\hat{\boldsymbol{L}} + \lambda^{-1}\boldsymbol{I}; (\boldsymbol{\Pi}_1\hat{\boldsymbol{B}})_j^\top)$. Similarly we denote $\boldsymbol{\Pi}_{\mathcal{S}}$ as the matrix with j-th row equals to $\mathsf{SSolve}_{2^{1/4}}(\hat{\boldsymbol{L}} + \lambda^{-1}\boldsymbol{I}; (\boldsymbol{\Pi}_2)_j^\top)$. By using Lemma A.1 to both solvers we have

$$\|\boldsymbol{B}_{\mathcal{S}}\hat{\boldsymbol{b}}_i\|^2 + \lambda^{-1}\|\boldsymbol{\Pi}_{\mathcal{S}}\hat{\boldsymbol{b}}_i\|^2 \approx_{\sqrt{2}-1} \|\boldsymbol{\Pi}_1\hat{\boldsymbol{B}}(\hat{\boldsymbol{L}} + \lambda^{-1}\boldsymbol{I})^{-1}\hat{\boldsymbol{b}}_i\|^2 + \lambda^{-1}\|\boldsymbol{\Pi}_2(\hat{\boldsymbol{L}} + \lambda^{-1}\boldsymbol{I})^{-1}\hat{\boldsymbol{b}}_i\|^2 \tag{C.42}$$

for all $i \in \{1, 2, \cdots, m\}$. By eq.(C.41) and eq.(C.42), if we set $\tilde{l}_i := \|\boldsymbol{B}_{\mathcal{S}}\hat{\boldsymbol{b}}_i\|^2 + \lambda^{-1}\|\boldsymbol{\Pi}_{\mathcal{S}}\hat{\boldsymbol{b}}_i\|^2$, then with probability $1 - \frac{1}{4n}$, we obtain all the approximation of ridge leverage scores $\{\tilde{l}_i\}_{i=1}^m$ such that $\tilde{l}_i \approx_{1/2} l_i$ holds for all i. Notice that since $\boldsymbol{B}_{\mathcal{S}}, \boldsymbol{\Pi}_{\mathcal{S}} \in \mathbb{R}^{k\times n}$, and that each $\hat{\boldsymbol{b}}_i$ only contains 2 non-zero entries, thus it takes $\tilde{O}(k \cdot m)$ to pre-compute $\boldsymbol{B}_{\mathcal{S}}$ and $\boldsymbol{\Pi}_{\mathcal{S}}$, and takes $O(2k \cdot m)$ to compute $\{\boldsymbol{B}_{\mathcal{S}}\hat{\boldsymbol{b}}_i, \boldsymbol{\Pi}_{\mathcal{S}}\hat{\boldsymbol{b}}_i\}_{i=1}^m$. To summarize, computing all $\tilde{l}_i$ takes $\tilde{O}(km) = \tilde{O}(m \log m) = \tilde{O}(m)$. With these ridge leverage score approximations, we apply Lemma C.4 to matrix $\hat{\boldsymbol{B}}$ with choice $\delta = 1/4n$. By setting $\tilde{\boldsymbol{L}} := \hat{\boldsymbol{B}}^\top\boldsymbol{S}^\top\boldsymbol{S}\hat{\boldsymbol{B}}$ we have $\tilde{\boldsymbol{L}} + \lambda^{-1}\boldsymbol{I} \approx_\epsilon \hat{\boldsymbol{L}} + \lambda^{-1}\boldsymbol{I}$ holds with probability $1 - 1/4n$. By applying another union bound we obtain our final result:

$$\tilde{\boldsymbol{L}} + \lambda^{-1}\boldsymbol{I} \approx_\epsilon \hat{\boldsymbol{L}} + \lambda^{-1}\boldsymbol{I} \quad \text{with probability} \quad 1 - \frac{1}{2n}. \tag{C.43}$$

Finally, according to Lemma C.4, the number of edges of $\tilde{\boldsymbol{L}}$ is $s = Cn_\lambda \log(n^2)/\epsilon^2 = O(n_\lambda \log n/\epsilon^2)$. Since the last step of computing $\tilde{\boldsymbol{L}} = (\boldsymbol{S}\hat{\boldsymbol{B}})^\top(\boldsymbol{S}\hat{\boldsymbol{B}})$ only takes $O(s) = \tilde{O}(n_\lambda/\epsilon^2)$ due to the sparsity of $\hat{\boldsymbol{B}}$, the overall time complexity of Algorithm 2 is $\tilde{O}(m + n_\lambda/\epsilon^2)$.

Lemma C.3 (Johnson–Lindenstrauss, [12])**.** *Let $\boldsymbol{\Pi} \in \mathbb{R}^{k\times n}$ be Gaussian sketch matrix with each entry independent and equal to $\mathcal{N}(0, 1/k)$ where $\mathcal{N}(0, 1)$ denotes a standard Gaussian random variable. If we choose $k = O\left(\frac{\log(1/\delta)}{\epsilon^2}\right)$, then for any vector $\boldsymbol{x} \in \mathbb{R}^n$, with probability $1 - \delta$ we have*

$$(1 - \epsilon)\|\boldsymbol{x}\| \le \|\boldsymbol{\Pi}\boldsymbol{x}\| \le (1 + \epsilon)\|\boldsymbol{x}\|. \tag{C.44}$$

Lemma C.4 (Spectral approximation, [11])**.** *Let $\boldsymbol{S}$ be an $s \times m$ subsampling matrix with probabilities $p_i = \tilde{\ell}_i/Z$ where $\tilde{\ell}_i \approx_{1/2} \ell_i$ and Z is the normalization constant. If we have $s \ge Cn_\lambda \log(n/\delta)/\epsilon^2$ for some constant $C > 0$ and $\epsilon, \delta \in (0, 1/2]$, then we have*

$$\hat{\boldsymbol{B}}^\top\boldsymbol{S}^\top\boldsymbol{S}\hat{\boldsymbol{B}} + \lambda^{-1}\boldsymbol{I} \approx_\epsilon \hat{\boldsymbol{B}}^\top\hat{\boldsymbol{B}} + \lambda^{-1}\boldsymbol{I} \tag{C.45}$$

holds with probability $1 - \delta$. Here $n_\lambda = \mathrm{Tr}[\hat{\boldsymbol{L}}(\hat{\boldsymbol{L}} + \lambda^{-1}\boldsymbol{I})^{-1}]$.

C.5 Proof of Lemma 5.3

We first prove a lemma which is related to the approximation rate of squared matrices.

Lemma C.5. *Suppose that $\mathbf{\Sigma}$ and $\widetilde{\mathbf{\Sigma}}$ are two $n \times n$ PD matrices, and $\widetilde{\mathbf{\Sigma}} \approx_{\frac{\beta}{\kappa}} \mathbf{\Sigma}$, where κ is the condition number of $\mathbf{\Sigma}$ and $\beta \in \left(0, \frac{1}{8}\right)$, then we have*

$$\widetilde{\mathbf{\Sigma}}^2 \approx_{8\beta} \mathbf{\Sigma}^2. \tag{C.46}$$

Proof. Let $\epsilon = \frac{\beta}{\kappa}$. The condition $\mathbf{\Sigma} \approx_\epsilon \widetilde{\mathbf{\Sigma}}$ implies that $\left\|\mathbf{\Sigma} - \widetilde{\mathbf{\Sigma}}\right\| \leq \epsilon \|\mathbf{\Sigma}\|$. We have

$$\begin{aligned}
\left\|\left(\mathbf{\Sigma} - \widetilde{\mathbf{\Sigma}}\right)\boldsymbol{x}\right\| &= \left\|\left(\mathbf{\Sigma} - \widetilde{\mathbf{\Sigma}}\right)\mathbf{\Sigma}^{-1}\mathbf{\Sigma}\boldsymbol{x}\right\| && \text{(C.47)}\\
&\leq \left\|\left(\mathbf{\Sigma} - \widetilde{\mathbf{\Sigma}}\right)\mathbf{\Sigma}^{-1}\right\| \times \|\mathbf{\Sigma}\boldsymbol{x}\| && \text{(C.48)}\\
&\leq \left\|\left(\mathbf{\Sigma} - \widetilde{\mathbf{\Sigma}}\right)\right\| \left\|\mathbf{\Sigma}^{-1}\right\| \times \|\mathbf{\Sigma}\boldsymbol{x}\| && \text{(C.49)}\\
&\leq \epsilon \|\mathbf{\Sigma}\| \left\|\mathbf{\Sigma}^{-1}\right\| \times \|\mathbf{\Sigma}\boldsymbol{x}\| && \text{(C.50)}\\
&= \epsilon\kappa \|\mathbf{\Sigma}\boldsymbol{x}\| && \text{(C.51)}\\
&= \beta \|\mathbf{\Sigma}\boldsymbol{x}\|. && \text{(C.52)}
\end{aligned}$$

For any $\boldsymbol{x} \in \mathbb{R}^n$, by triangle inequality we have

$$\|\mathbf{\Sigma}\boldsymbol{x}\| - \left\|\left(\mathbf{\Sigma} - \widetilde{\mathbf{\Sigma}}\right)\boldsymbol{x}\right\| \leq \left\|\widetilde{\mathbf{\Sigma}}\boldsymbol{x}\right\| \leq \|\mathbf{\Sigma}\boldsymbol{x}\| + \left\|\left(\mathbf{\Sigma} - \widetilde{\mathbf{\Sigma}}\right)\boldsymbol{x}\right\|. \tag{C.53}$$

Subtracting the inequality $\left\|\left(\mathbf{\Sigma} - \widetilde{\mathbf{\Sigma}}\right)\boldsymbol{x}\right\| \leq \beta \|\mathbf{\Sigma}\boldsymbol{x}\|$ we derived before into eq.(C.53) and squaring all sides, we have

$$(1-\beta)^2 \boldsymbol{x}^\top \mathbf{\Sigma}^2 \boldsymbol{x} \leq \boldsymbol{x}^\top \widetilde{\mathbf{\Sigma}}\boldsymbol{x} \leq (1+\beta)^2 \boldsymbol{x}^\top \mathbf{\Sigma}^2 \boldsymbol{x}. \tag{C.54}$$

Since $0 < \beta < \frac{1}{8}$, the claim is proved. □

Let $\boldsymbol{T} = \boldsymbol{X}^\top \left(\boldsymbol{I} + \lambda\hat{\boldsymbol{L}}\right)^{-2} \boldsymbol{X}$ be the true Hessian. Let $\tilde{\boldsymbol{T}} = \boldsymbol{X}^\top \left(\boldsymbol{I} + \lambda\tilde{\boldsymbol{L}}\right)^{-2} \boldsymbol{X}$ be the approximated Hessian using sparsified Laplacian $\tilde{\boldsymbol{L}}$. By Lemma 5.2, $\boldsymbol{I} + \lambda\tilde{\boldsymbol{L}} \approx_{\frac{\beta}{3\lambda}} \boldsymbol{I} + \lambda\boldsymbol{L}$ with probability at least $1 - \frac{1}{2n}$. From Lemma C.5, we have $\tilde{\boldsymbol{T}} \approx_{8\beta} \boldsymbol{T}$.

Next, we show that $\boldsymbol{Q}^\top\boldsymbol{Q} \approx_{O(\beta)} \boldsymbol{T}$. Let $\tilde{\boldsymbol{H}} = \boldsymbol{I} + \lambda\tilde{\boldsymbol{L}}$. Let $\mathcal{S}$ be the operator defined by $\mathsf{SSolve}_{\frac{\beta}{\sqrt{3\lambda}}}\left(\tilde{\boldsymbol{H}}, \cdot\right)$, i.e. $\boldsymbol{q}_j = \mathcal{S}(\boldsymbol{x}_j)$ where $\boldsymbol{q}_j$ and $\boldsymbol{x}_j$ are the j-th column of $\boldsymbol{Q}$ and $\boldsymbol{X}$ respectively. From Lemma A.1 we have for any $\boldsymbol{z} \in \mathbb{R}^d$,

$$\begin{aligned}
\left\|\boldsymbol{Q}\boldsymbol{z} - \tilde{\boldsymbol{H}}^{-1}\boldsymbol{X}\boldsymbol{z}\right\|_2^2 &= \left\|\sum_{j=1}^d z_j \left(\mathcal{S}(\boldsymbol{x}_j) - \tilde{\boldsymbol{H}}\boldsymbol{x}_j\right)\right\|_2^2 && \text{(C.55)}\\
&= \left\|\mathcal{S}\left(\sum_{j=1}^d z_j\boldsymbol{x}_j\right) - \tilde{\boldsymbol{H}}\left(\sum_{j=1}^d z_j\boldsymbol{x}_j\right)\right\|_2^2 && \text{(C.56)}\\
&\leq \frac{\beta^2}{3\lambda}\left\|\tilde{\boldsymbol{H}}^{-1}\boldsymbol{X}\boldsymbol{z}\right\|_{\tilde{\boldsymbol{H}}}^2 && \text{(C.57)}\\
&\leq \beta^2 \|\tilde{\boldsymbol{H}}^{-1}\boldsymbol{X}\boldsymbol{z}\|_2^2. && \text{(C.58)}
\end{aligned}$$

Therefore we have

$$(1-\beta)\|\tilde{\boldsymbol{H}}^{-1}\boldsymbol{X}\boldsymbol{z}\|_2 \leq \|\boldsymbol{Q}\boldsymbol{z}\| \leq (1+\beta)\|\tilde{\boldsymbol{H}}^{-1}\boldsymbol{X}\boldsymbol{z}\|_2, \tag{C.59}$$

and this is equivalent to

$$(1-\beta)^2\boldsymbol{z}^\top(\boldsymbol{X}\tilde{\boldsymbol{H}}^{-2}\boldsymbol{X})\boldsymbol{z} \leq \boldsymbol{z}^\top\boldsymbol{Q}^\top\boldsymbol{Q}\boldsymbol{z} \leq (1+\beta)^2\boldsymbol{z}^\top\left(\boldsymbol{X}^\top\tilde{\boldsymbol{H}}^{-2}\boldsymbol{X}\right)\boldsymbol{z}. \tag{C.60}$$

Notice that $\boldsymbol{X}^\top\tilde{\boldsymbol{H}}^{-2}\boldsymbol{X} = \tilde{\boldsymbol{T}}$. We conclude that $\boldsymbol{Q}^\top\boldsymbol{Q} \approx_{2\beta+\beta^2} \tilde{\boldsymbol{T}}$. When $\beta < \frac{1}{8}$, we have $\boldsymbol{Q}^\top\boldsymbol{Q} \approx_{4\beta} \tilde{\boldsymbol{T}}$.

Lastly, from Lemma A.2 and the discussions in Appendix A.3, we have there exists a constant $C' \in (0, 1/4)$, such that

$$\boldsymbol{P} = \tilde{\boldsymbol{Q}}^\top\tilde{\boldsymbol{Q}} \approx_{C'} \boldsymbol{Q}^\top\boldsymbol{Q} \tag{C.61}$$

with probability at least $1 - \frac{1}{2n}$.

Put the results above together and we get

$$\boldsymbol{P} \approx_{12\beta+C'} \boldsymbol{T}. \tag{C.62}$$

Notice that $12\beta + C' < \frac{1}{2}$. Using a union bound can prove that the fail probability of this whole process is bounded by $\frac{1}{n}$.

C.6 Proof of Lemma 5.4

Let $\boldsymbol{F} = (\boldsymbol{I} + \lambda\hat{\boldsymbol{L}})\boldsymbol{X}$. We have the Hessian of ℓ' is

$$\nabla^2\ell' = \boldsymbol{P}^{-\frac{1}{2}}\boldsymbol{F}^\top\boldsymbol{F}\boldsymbol{P}^{-\frac{1}{2}}. \tag{C.63}$$

From the condition that $\boldsymbol{P} \approx_{c_0} \boldsymbol{F}^\top\boldsymbol{F}$, we have $\boldsymbol{F}^\top\boldsymbol{F} \preceq (1+c_0)\boldsymbol{P}$, which implies

$$\boldsymbol{P}^{-1/2}\boldsymbol{F}^\top\boldsymbol{F}\boldsymbol{P}^{-1/2} \preceq (1+c_0)\boldsymbol{I}. \tag{C.64}$$

Similarly, since $\boldsymbol{P} \preceq (1+c_0)\boldsymbol{F}^\top\boldsymbol{F}$, we have

$$\left(\boldsymbol{F}^\top\boldsymbol{F}\right)^{-1} \preceq (1+c_0)\boldsymbol{P}^{-1}, \tag{C.65}$$

which implies

$$\left[\lambda_{\min}(\boldsymbol{P}^{-1/2}\boldsymbol{F}^\top\boldsymbol{F}\boldsymbol{P}^{-1/2})\right]^{-1} = \lambda_{\max}\left(\boldsymbol{P}^{1/2}\left(\boldsymbol{F}^\top\boldsymbol{F}\right)^{-1}\boldsymbol{P}^{1/2}\right) \tag{C.66}$$

$$\leq 1 + c_0. \tag{C.67}$$

.

Notice that ℓ' and ℓ have the same global optimal value, let it be ℓ^*. For any $\boldsymbol{w}'$ satisfies $\ell'(\boldsymbol{w}') - \ell^* \leq \gamma$, we have

$$\ell\left(\boldsymbol{P}^{1/2}\boldsymbol{w}'\right) - \ell^* = \ell'(\boldsymbol{w}') - \ell^* \leq \gamma. \tag{C.68}$$

Therefore, if $\boldsymbol{w}'$ is a solution of ℓ' with ϵ error rate, then $\boldsymbol{P}^{1/2}\boldsymbol{w}'$ is a solution of ℓ with ϵ error rate.

C.7 Proof of Theorem 5.1

As we noted in the main paper, Algorithm 1 is composed by two components: constructing the preconditioner $\boldsymbol{P}$ and applying it to the optimization.

Constructing the Preconditioner. From Lemma 5.2, the first step that applies spectral sparsifier to get $\tilde{\boldsymbol{L}}$ requires $\tilde{O}(m)$ time and the number of non-zero entries in $\tilde{\boldsymbol{L}}$ is $\tilde{O}\left(n_\lambda\lambda^2\right)$. By Lemma A.1, running the SDD solver with error rate $\frac{\beta}{3\lambda}$ in the second step requires $\tilde{O}\left(n_\lambda\lambda^2\right)$ time. Notice that since $\boldsymbol{X}$ is an $n \times d$ matrix, we actually need to run SDD solver for d times, and this introduces another d factor in the time complexity.

As we noted in Appendix A.3, applying the Hadamard transformation to $\boldsymbol{RQ}$ requires $\tilde{O}(d)$ time, and applying the subsampling requires $\tilde{O}(n)$ time. Since $\tilde{\boldsymbol{Q}} \in \mathbb{R}^{s\times d}$, calculating $\boldsymbol{P} = \tilde{\boldsymbol{Q}}^\top\boldsymbol{Q}$ requires $O(d^2 s)$ time. Since $s = \tilde{O}(d)$, this step takes $\tilde{O}(d^3)$ time. We use brute force to calculate $\boldsymbol{P}' = \boldsymbol{P}^{-1/2}$, and this takes $O(d^3)$ time.

As a summary, constructing the preconditioner $\boldsymbol{P}'$ takes $\tilde{O}(n_\lambda\lambda^2 d + nd + d^3)$ time. Notice that we only perform this step once during the whole algorithm.

Performing the Iterations. Next we consider the time required for each iteration. We calculate $\boldsymbol{u}^{(t)}$ from right to left and it takes $O(nd)$ time. Next, we need to perform two SDD solvers with error rate μ. From Lemma A.1, it takes $\tilde{O}\left[m\log\left(\frac{1}{\mu}\right)\right]$, which is $\tilde{O}\left[m\log\left(\frac{1}{\epsilon}\right)\right]$. Calculating $\boldsymbol{g}^{(t)}$ and $\boldsymbol{w}^{(t)}$ is straight-forward and takes $\tilde{O}(nd)$ time.

To conclude, performing each iteration requires $\tilde{O}\left[m\log\left(\frac{1}{\epsilon}\right)+nd\right]$ time. By Lemma 5.1 and Lemma 5.3, with a proper step size, the number of iterations needed for solving outer problem is $\tilde{O}\left(\log 1/\epsilon\right)$.

Combining the analysis above together, to overall complexity is

$$\tilde{O}\left[n_\lambda\lambda^2 d+nd+d^3+\left(m\log\left(\frac{1}{\epsilon}\right)+nd\right)\log\left(\frac{1}{\epsilon}\right)\right]=\tilde{O}\left(n_\lambda\lambda^2 d+d^3+(m+nd)\left(\log 1/\epsilon\right)^2\right), \tag{C.69}$$

which proves the claim.

D Further Discussions

In this section, we extend some of the discussions in the main paper.

D.1 An Analysis of CE Loss v.s. MSE Loss

Although HERTA is derived from MSE loss, the experiment result shows it also works on CE loss. In this subsection we provide an analysis showing the similarity of the gradient and Hessian of TWIRLS on CE loss and MSE loss, to offer a intuitive explanation why a method that is derived from MSE loss can work on CE loss.

In this section, for a node $u\in\{1,2,\cdots,n\}$, we use $\boldsymbol{y}^{(u)}\in\mathbb{R}^c$ to represent the u-th row of $\boldsymbol{Y}$ (notice we use super-script here to distinguish from $\boldsymbol{y}_i$ used before), $\boldsymbol{h}_u\in\mathbb{R}^n$ to represent the u-th row of $\left(\boldsymbol{I}+\lambda\hat{\boldsymbol{L}}\right)^{-1}$. For $p\in\{1,2,\cdots d\}$, we use $\boldsymbol{x}_p\in\mathbb{R}^n$ to denote the p-th column of $\boldsymbol{X}$. For $i\in\{1,2,\cdots c\}$, we use $y_i^{(u)}$ to denote the i-th entry of $\boldsymbol{y}^{(u)}$ (or in other words the (u,i)-th entry of $\boldsymbol{Y}$), and $w_{p,i}$ to denote the (p,i)-th entry of $\boldsymbol{W}$.

The MSE loss of TWIRLS can be decomposed into summation of sub-losses of each node, i.e.

$$\ell(\boldsymbol{W})=\sum_{u=1}^{n}\frac{1}{2}\left\|\boldsymbol{h}_u^\top\boldsymbol{X}\boldsymbol{W}-\boldsymbol{y}^{(u)}\right\|_{\mathcal{F}}^2=\sum_{u=1}^{n}\ell^{(u)}\left(\boldsymbol{W}\right), \tag{D.1}$$

where $\ell^{(u)}(\boldsymbol{W})=\frac{1}{2}\left\|\boldsymbol{W}^\top\boldsymbol{X}^\top\boldsymbol{h}_u-\boldsymbol{y}^{(u)}\right\|_{\mathcal{F}}^2$. For a specific class $i\in\{1,2,\cdots,c\}$, we have the gradient of $\ell^{(u)}$ w.r.t. $\boldsymbol{w}_i$ is

$$\frac{\partial\ell^{(u)}}{\partial\boldsymbol{w}_i}=\boldsymbol{X}^\top\boldsymbol{h}_u\boldsymbol{h}_u^\top\boldsymbol{X}\boldsymbol{w}_i-\boldsymbol{X}^\top\boldsymbol{h}_u\times y_i^{(u)}. \tag{D.2}$$

It is not hard to see from eq.(D.2) that the Hessian of $\ell^{(u)}$ with respect to $\boldsymbol{w}_i$ is

$$\nabla^2_{\boldsymbol{w}_i}\ell^{(u)}\left(\boldsymbol{W}\right)=\boldsymbol{X}^\top\boldsymbol{h}_u\boldsymbol{h}_u^\top\boldsymbol{X}. \tag{D.3}$$

For classification tasks, the target $\boldsymbol{y}^{(u)}$-s are one-hot vectors representing the class of the node. Notice when we calculate cross entropy loss, we use $\mathsf{softmax}$ to normalize it before feeding it into the loss function. In the following for a vector $\boldsymbol{v}\in\mathbb{R}^c$ whose i-th entry is v_i, we define

$$\mathsf{softmax}(\boldsymbol{v})_i=\frac{\exp(v_i)}{\sum_{j=1}^{c}\exp(v_j)}. \tag{D.4}$$

Suppose the u-th node belongs to class k, then the cross entropy loss of the u-th node is defined as

$$\mathsf{CE}^{(u)}(\boldsymbol{W})=-\log\mathsf{softmax}\left(\boldsymbol{h}_u^\top\boldsymbol{X}\boldsymbol{W}\right)_k \tag{D.5}$$

$$=-\boldsymbol{h}_u^\top\boldsymbol{X}\boldsymbol{w}_k+\log\sum_{j=1}^{c}\exp\left(\boldsymbol{h}_u^\top\boldsymbol{X}\boldsymbol{w}_j\right), \tag{D.6}$$

The gradient of $\mathsf{CE}^{(u)}$ w.r.t. $\boldsymbol{w}_i$ is

$$\frac{\partial \mathsf{CE}^{(u)}}{\partial \boldsymbol{w}_i} = -\boldsymbol{\delta}_{i,k} \times \boldsymbol{X}^\top \boldsymbol{h}_u + \frac{\boldsymbol{X}^\top \boldsymbol{h}_u \exp\left(\boldsymbol{h}_u^\top \boldsymbol{X} \boldsymbol{w}_i\right)}{\sum_{j=1}^c \exp\left(\boldsymbol{h}_u^\top \boldsymbol{X} \boldsymbol{w}_j\right)} \tag{D.7}$$

$$= \boldsymbol{X}^\top \boldsymbol{h}_u \mathrm{softmax}\left(\boldsymbol{h}_u^\top \boldsymbol{X} \boldsymbol{W}\right)_i - \boldsymbol{X}^\top \boldsymbol{h}_u \times y_i^{(u)}. \tag{D.8}$$

By taking another partial differentiation, we have

$$\frac{\partial^2 \mathsf{CE}^{(u)}}{\partial w_{p,i} \partial w_{q,i}} = \frac{\left(\boldsymbol{x}_p^\top \boldsymbol{h}_u\right)\left(\boldsymbol{x}_q^\top \boldsymbol{h}_u\right) \exp\left(\boldsymbol{h}_u^\top \boldsymbol{X} \boldsymbol{w}_i\right)}{\sum_{j=1}^c \exp\left(\boldsymbol{h}_u^\top \boldsymbol{X} \boldsymbol{w}_j\right)} - \frac{\left(\boldsymbol{x}_p^\top \boldsymbol{h}_u\right)\left(\boldsymbol{x}_q^\top \boldsymbol{h}_u\right) \left[\exp\left(\boldsymbol{h}_u^\top \boldsymbol{X} \boldsymbol{w}_i\right)\right]^2}{\left[\sum_{j=1}^c \exp\left(\boldsymbol{h}_u^\top \boldsymbol{X} \boldsymbol{w}_j\right)\right]^2} \tag{D.9}$$

$$= \left(\boldsymbol{x}_p^\top \boldsymbol{h}_u\right)\left(\boldsymbol{x}_q^\top \boldsymbol{h}_u\right)\left[s_i - s_i^2\right], \tag{D.10}$$

where $s_i = \mathsf{softmax}\left(\boldsymbol{h}_u^\top \boldsymbol{X} \boldsymbol{W}\right)_i$. Rewriting eq.(D.10) into matrix form, we have

$$\nabla^2_{\boldsymbol{w}_i} \mathsf{CE}^{(u)}(\boldsymbol{W}) = (s_i - s_i^2) \boldsymbol{X}^\top \boldsymbol{h}_u \boldsymbol{h}_u^\top \boldsymbol{X}. \tag{D.11}$$

Comparing eq.(D.2) and eq.(D.8), we can notice that the gradient of MSE loss and CE loss are essentially the same except the term $\boldsymbol{h}_u^\top \boldsymbol{X} \boldsymbol{w}_i$ in eq.(D.2) is normalized by softmax in eq.(D.8). Additionally, by comparing the Hessian of MSE loss eq.(D.3) and the Hessian of CE loss eq.(D.11), we have the latter is a rescaled version of the former. These similarities intuitively explains why our method can be also used on CE loss.

D.2 The Unavoidable λ^2 in the Running Time

Lemma C.5 essentially states the following idea: even when two PD matrices are very similar (in terms of spectral approximation), if they are ill-conditioned, their square can be very different. In this subsection, we prove that the bound obtained in Lemma C.5 is strict up to constant factors by explicitly constructing a worst case. Notice that, in this subsection we discuss the issue of squaring spectral approximators in a broader context, thus in this subsection we possibly overload some symbols used before to simplify the notation.

First we consider another definition of approximation rate: for two PD matrices $\boldsymbol{\Sigma}$ and $\widetilde{\boldsymbol{\Sigma}}$, we define the approximation rate as

$$\psi\left(\boldsymbol{\Sigma}, \widetilde{\boldsymbol{\Sigma}}\right) = \max\left\{\left\|\boldsymbol{\Sigma}^{-1/2} \widetilde{\boldsymbol{\Sigma}} \boldsymbol{\Sigma}^{-1/2}\right\|, \left\|\widetilde{\boldsymbol{\Sigma}}^{-1/2} \boldsymbol{\Sigma} \widetilde{\boldsymbol{\Sigma}}^{-1/2}\right\|\right\}. \tag{D.12}$$

This definition is easier to calculate in the scenario considered in this subsection, and can be easily translated to the definition we used in Section 3: when $\epsilon = \psi\left(\boldsymbol{\Sigma}, \widetilde{\boldsymbol{\Sigma}}\right) \in (0, 1)$, we have $\widetilde{\boldsymbol{\Sigma}} \approx_\epsilon \boldsymbol{\Sigma}$, and when $\psi\left(\boldsymbol{\Sigma}, \widetilde{\boldsymbol{\Sigma}}\right)$ is larger than 1 we don't have an approximation in the form defined in Section 3.

Let $\gamma > 1$ and $\delta \in (0, 1)$ be real numbers. Define

$$\boldsymbol{\Sigma} = \begin{bmatrix} 1 & 0 \\ 0 & 1 \end{bmatrix} \begin{bmatrix} \gamma & 0 \\ 0 & 1 \end{bmatrix} \begin{bmatrix} 1 & 0 \\ 0 & 1 \end{bmatrix}, \tag{D.13}$$

and

$$\widetilde{\boldsymbol{\Sigma}} = \begin{bmatrix} \sqrt{1-\delta^2} & -\delta \\ \delta & \sqrt{1-\delta^2} \end{bmatrix} \begin{bmatrix} \gamma & 0 \\ 0 & 1 \end{bmatrix} \begin{bmatrix} \sqrt{1-\delta^2} & \delta \\ -\delta & \sqrt{1-\delta^2} \end{bmatrix}. \tag{D.14}$$

It's not hard to compute the error rate $\psi\left(\boldsymbol{\Sigma}, \widetilde{\boldsymbol{\Sigma}}\right) = \left\|\boldsymbol{\Sigma}^{-1/2} \widetilde{\boldsymbol{\Sigma}} \boldsymbol{\Sigma}^{-1/2}\right\| \approx \Theta(\gamma \delta^2)$. While if we consider the squared matrices, we have $\psi\left(\boldsymbol{\Sigma}^2, \widetilde{\boldsymbol{\Sigma}}^2\right) = \left\|\boldsymbol{\Sigma}^{-1} \widetilde{\boldsymbol{\Sigma}}^2 \boldsymbol{\Sigma}^{-1}\right\| \approx \gamma^2 \delta^2$. In this case, $\psi\left(\boldsymbol{\Sigma}^2, \widetilde{\boldsymbol{\Sigma}}^2\right)$ is larger than $\psi\left(\boldsymbol{\Sigma}, \widetilde{\boldsymbol{\Sigma}}\right)$ by a factor of γ, which is the condition number of $\boldsymbol{\Sigma}$. When γ is very large and δ is very small, we can have a small $\psi\left(\boldsymbol{\Sigma}, \widetilde{\boldsymbol{\Sigma}}\right)$ while large $\psi\left(\boldsymbol{\Sigma}^2, \widetilde{\boldsymbol{\Sigma}}^2\right)$, which .

A More General Construction. For a PD matrix $\boldsymbol{\Sigma}$ and its spectral approximation $\widetilde{\boldsymbol{\Sigma}}$, we call $\frac{\psi(\boldsymbol{\Sigma}^2, \widetilde{\boldsymbol{\Sigma}}^2)}{\psi(\boldsymbol{\Sigma}, \widetilde{\boldsymbol{\Sigma}})}$ the Squared Error Rate. As noted above, in the worst case the squared error rate can be as large as the condition number of $\boldsymbol{\Sigma}$. However, the construction above is limited to 2×2 matrices. Now we construct a more general worst case of the squared error rate and perform a loose analysis. Although not rigorously proved, the construction and the analysis suggest the origination of large squared error rates: it approaches the upper bound (condition number) when the eigenspace of the two matrices are very well aligned but not exactly the same.

Let $\boldsymbol{A}$ be an ill-conditioned matrix with all eigenvalues very large except one eigenvalue equals to 1, and the eigenvalues of $\boldsymbol{B}$ are all closed to the eigenvalues of $\boldsymbol{A}$. Specifically, Let the SVD of $\boldsymbol{A}$ be $\boldsymbol{A} = \boldsymbol{U}\mathrm{diag}(\boldsymbol{\lambda})\boldsymbol{U}^\top$, where $\boldsymbol{\lambda} = [\lambda_1 \quad \lambda_2 \quad \cdots \lambda_n]$, and suppose $\lambda_n = 1$ and $\lambda_k \gg 1, \forall k \leq n-1$. For simplicity we just let $\boldsymbol{A}$ and $\boldsymbol{B}$ have the same eigenvalues. Suppose the SVD of $\boldsymbol{B}$ is $\boldsymbol{B} = \boldsymbol{V}\mathrm{diag}(\boldsymbol{\lambda})\boldsymbol{V}^\top$ and let $\boldsymbol{\Lambda} = \mathrm{diag}(\boldsymbol{\lambda})$. We denote the one sided error rate of $\boldsymbol{A}$ and $\boldsymbol{B}$ by ϵ, i.e. $\epsilon = \left\|\boldsymbol{A}^{-1/2}\boldsymbol{B}\boldsymbol{A}^{-1/2}\right\|$. We have

$$\epsilon = \left\|\boldsymbol{\Lambda}^{-1/2}\boldsymbol{U}^\top\boldsymbol{V}\boldsymbol{\Lambda}\boldsymbol{V}^\top\boldsymbol{U}\boldsymbol{\Lambda}^{-1/2}\right\| \tag{D.15}$$

$$= \left\|\boldsymbol{\Lambda}^{-1/2}\boldsymbol{W}\boldsymbol{\Lambda}\boldsymbol{W}^\top\boldsymbol{\Lambda}^{-1/2}\right\|, \tag{D.16}$$

where $\boldsymbol{W} = \boldsymbol{U}^\top\boldsymbol{V}$.

Since $\lambda_n = 1$ and for all $k \leq n-1$, $\lambda_k \gg 1$, we have

$$\boldsymbol{\Lambda}^{-\frac{1}{2}} = \begin{bmatrix} \lambda_1^{-1/2} & & & \\ & \lambda_2^{-\frac{1}{2}} & & \\ & & \ddots & \\ & & & \lambda_n^{-\frac{1}{2}} \end{bmatrix} \approx \begin{bmatrix} 0 & & & \\ & 0 & & \\ & & \ddots & \\ & & & 1 \end{bmatrix}, \tag{D.17}$$

and therefore

$$\epsilon = \left\|\boldsymbol{\Lambda}^{-1/2}\boldsymbol{W}\boldsymbol{\Lambda}\boldsymbol{W}^\top\boldsymbol{\Lambda}^{-1/2}\right\| \approx (\boldsymbol{W}\boldsymbol{\Lambda}\boldsymbol{W}^\top)_{n,n} = \sum_{k=1}^{n} \boldsymbol{W}_{k,n}^2\lambda_k, \tag{D.18}$$

where $\boldsymbol{A}_{i,j}$ represents the (i,j)-th entry of a matrix $\boldsymbol{A}$.

For simplicity, we assume all $\lambda_k (k \leq n-1)$ are approximate equal, i.e. $\lambda_1 \approx \lambda_2 \cdots \approx \lambda_{n-1} = \gamma$. Then we have

$$\epsilon = \sum_{k=1}^{n} \boldsymbol{W}_{k,n}^2\lambda_k \tag{D.19}$$

$$\approx \gamma\left[\sum_{k=1}^{n-1} \boldsymbol{W}_{k,n}^2 + \frac{1}{\gamma}\boldsymbol{W}_{n,n}^2\right] \tag{D.20}$$

$$\approx \gamma\sum_{k=1}^{n-1} \boldsymbol{W}_{k,n}^2 \tag{D.21}$$

$$= \gamma\left(1 - \boldsymbol{W}_{n,n}^2\right). \tag{D.22}$$

Recall $\boldsymbol{W} = \boldsymbol{U}^\top\boldsymbol{V}$, we have $\boldsymbol{W}_{n,n} = \boldsymbol{u}_n^\top\boldsymbol{v}_n$, where $\boldsymbol{u}_n$ and $\boldsymbol{v}_n$ are the n-th column of $\boldsymbol{U}$ and $\boldsymbol{V}$ respectively. Thus we have

$$\epsilon \approx \gamma\left[1 - \left(\boldsymbol{u}_n^\top\boldsymbol{v}_n\right)^2\right]. \tag{D.23}$$

Now we can see the spectral approximation error ϵ is determined by two terms: the condition number γ and the matchness of the eigenvectors corresponds to small eigenvalues, which is evaluated by $\left[1 - \left(\boldsymbol{u}_n^\top\boldsymbol{v}_n\right)^2\right]$. **When γ is very large but $\left[1 - \left(\boldsymbol{u}_n^\top\boldsymbol{v}_n\right)^2\right]$ is small, B can still be a spectral approximation of $\boldsymbol{A}$**. For example if $(1 - \boldsymbol{u}_n^\top\boldsymbol{v}_n) \approx \gamma^{-1}$, we can get a spectral approximation error $\epsilon \approx 1$. However, after we square the matrices, the eigenvalues will also get squared, but eigenvectors remains unchanged. That will enlarge the spectral approximation error by a factor of γ, i.e. $\left\|\boldsymbol{A}^{-1}\boldsymbol{B}^2\boldsymbol{A}^{-1}\right\| \approx \gamma^2\gamma^{-1} = \gamma$, which becomes very large. In this case the squared error rate is γ, the condition number of $\boldsymbol{A}$.

D.3 Applying Graph Sparsification in Each Iteration

As mentioned in the main paper, unlike most existing work, in our algorithm we don't sparsify the graph in each training iteration. The proof of Lemma 5.1 (see Appendix C.3) suggests the reason why performing graph sparsification in each iteration can lead to suboptimal running time. In this subsection we illustrate this claim in detail. The intuition is that, in order to ensure convergence of the training, we require a small error rate in the gradient estimation, which is of the order $\epsilon^{1/2}$ as we have showed in Appendix C.3. It is acceptable for the SDD solver because the running time of the SDD solver only logarithmly depends on the error rate. However, if we sparsify the graph, to obtain an $\epsilon^{1/2}$ error rate we will need to sample $O(n_\lambda/\epsilon)$ edges, which grows linearly with $1/\epsilon$, and can be large especially when ϵ is very small. Below is a more detailed analysis.

Consider in the for-loop of Algorithm 1 we replace the $\hat{\boldsymbol{L}}$ by a sparsified version $\boldsymbol{L}' = \mathsf{Sparsify}_\omega\left(\hat{\boldsymbol{L}}\right)$, where $\omega \in (0,1)$. Let $\boldsymbol{H}' = \boldsymbol{I} + \lambda \boldsymbol{L}'$. From Lemma 5.2, we have $\boldsymbol{H}' \approx_\omega \boldsymbol{H}$. Consider E_1 defined in Appendix C.3, it now becomes

$$E_1' = \left\|\boldsymbol{X}^\top\left[\mathcal{S}\left(\boldsymbol{H}'^{-1}\boldsymbol{z}\right) - \boldsymbol{H}^{-2}\boldsymbol{z}\right]\right\| \tag{D.24}$$

$$\leq \sigma_{\max}\left(\boldsymbol{X}\right)\left\|\mathcal{S}\left(\boldsymbol{H}'^{-1}\boldsymbol{z}\right) - \boldsymbol{H}^{-2}\boldsymbol{z}\right\|. \tag{D.25}$$

Here we can not proceed by using the fact that $\mathcal{S}$ is a linear solver, because now $\mathcal{S}$ is not a linear solver for $\boldsymbol{H}$ but for $\boldsymbol{H}'$, thus we will have to split the error term again:

$$E_1' \leq \sigma_{\max}\left(\boldsymbol{X}\right)\left\|\mathcal{S}\left(\boldsymbol{H}'^{-1}\boldsymbol{z}\right) - \boldsymbol{H}'^{-2}\boldsymbol{z}\right\| + \sigma_{\max}(\boldsymbol{X})\left\|\boldsymbol{H}^{-2}\boldsymbol{z} + \boldsymbol{H}'^{-2}\boldsymbol{z}\right\|. \tag{D.26}$$

Of the two terms on the right-hand side of eq.(D.26), the first one can be bounded with a similar method used in Appendix C.3, and the second term is bounded by

$$\sigma_{\max}(\boldsymbol{X})\left\|\boldsymbol{H}^{-2}\boldsymbol{z} - \boldsymbol{H}'^{-2}\boldsymbol{z}\right\| \leq \sigma_{\max}\left(\boldsymbol{X}\right)\left\|I - \boldsymbol{H}^{-1}\boldsymbol{H}'^{-2}\boldsymbol{H}^{-1}\right\|\left\|\boldsymbol{H}^{-2}\boldsymbol{z}\right\| \tag{D.27}$$

$$\leq \sigma_{\max}\left(\boldsymbol{X}\right)\omega\left\|\boldsymbol{H}^{-2}\boldsymbol{z}\right\| \tag{D.28}$$

$$\leq \sqrt{\frac{8}{\epsilon}}\kappa(\boldsymbol{X})\lambda\omega\left\|\nabla\ell_i\left(\boldsymbol{w}\right)\right\|. \tag{D.29}$$

Therefore, in order to obtain $E_1' \leq \|\nabla\ell_i(\boldsymbol{w})\|$, we at least require $\omega \leq \frac{\epsilon^{-1/2}}{\sqrt{8}\kappa(\boldsymbol{X})\lambda} = O\left(\epsilon^{-1/2}\right)$. From Lemma 5.2, the number of edges in the sparsified graph ω error rate is $O(n_\lambda/\epsilon)$. A similar analysis can be also applied to E_2, and by repeating the proof in Appendix C.3, we obtain an overall running time bound

$$O(m + n_\lambda\lambda^2 d + d^3 + n_\lambda\epsilon^{-1}\log 1/\epsilon), \tag{D.30}$$

which, although eliminates the $m\left(\log\frac{1}{\epsilon}\right)^2$ term, introduces an extra $n_\lambda\epsilon^{-1}\log\frac{1}{\epsilon}$ term, and is usually worse than the original bound we derived in Theorem 5.1, especially when requiring a relatively small ϵ.

That being said, although not very likely, when ϵ and / or λ are large, it is possible that directly sparsifying the graph in each iteration is beneficial. Considering this, we can adopt a mixed strategy: when $n_\lambda\epsilon^{-1} \leq m\log(1/\epsilon)$, we sparsify the graph in each iteration, elsewise we don't. This leads to the following overall running time bound:

$$O\left[m + n_\lambda\lambda^2 d + d^3 + \min\left\{m\log\frac{1}{\epsilon}, n_\lambda\epsilon^{-1}\right\}\log\frac{1}{\epsilon}\right], \tag{D.31}$$

which is slightly better than the one we presented in Theorem 5.1.

D.4 Possible Directions for Extending HERTA to More Complex Models

The assumption that $f(\boldsymbol{X};\boldsymbol{W}) = \boldsymbol{X}\boldsymbol{W}$ provides us with a convenience that the Hessian of this model is a constant matrix. Therefore in Algorithm 1 we only need to calculate the preconditioner $\boldsymbol{P}$ for one time. However, if $f(\boldsymbol{X};\boldsymbol{W})$ is implemented by a non-linear network, then the Hessian will change by the time and might be hard to calculate, which will be a key challenge to using a more complex f. We note that this can be possibly addressed by constructing a linear approximation of f using its Jaccobian. In each iteration, we can use the Jaccobian to replace the $\boldsymbol{X}$ used in current

version of HERTA, and recalculate $\boldsymbol{P}$ at each iteration. Since the convergence is fast, we only need to recalculate the Jaccobian for a small number of iterations, so should not bring massive change to the running time of the algorithm.

The attention mechanism of TWIRLS in [46] is achieved by adding a concave penalty function to each summand of the the $\mathrm{Tr}\left(\boldsymbol{Z}^\top \hat{\boldsymbol{L}} \boldsymbol{Z}\right)$ term in eq.(4.1). For specific penalty functions, it might still possible to find a inner problem solver, as long as the problem stay convex. We note that this depends on concrete implementation of the penalty term used. Investigating how to fast solve the inner problem under various penalty functions should also be an important problem for future study.

E Implementation Details

In the experiments, the datasets are loaded and processed using the DGL package [40]. We use the original inner problem solver in [46] since it is not computation bottleneck. It can be in principle replaced by any implementation of SDD solvers.

For the calculating the gradient of the preconditioned model, we presented a calculation method in Algorithm 1 which maintains the lowest computational complexity. In preliminary experiments, we tested this calculation method with using the autograd module in pytorch[3] and verified that they have the same output, and similar computational efficiency on real world datasets (again in practice this step is not a bottleneck). Therefore, we simply use pytorch autograd module to compute gradients in experiments.

Using the pytorch autograd module also enables us to apply HERTA on various loss functions and optimizers: we only need to perform the preconditioning and indicate the loss function. The gradient and optimization algorithm with be automatically realized by pytorch.

In order to ensure a fair comparison and prevent confounding factors, we don't using any common training regularization techniques like weight decay or dropout. For each setting, we repeat the experiment with learning rates in $\{0.001, 0.01, 0.1, 1, 10\}$ and choose the trial which the training loss does not explode and with the lowest final training loss to report in the main paper.

F Additional Experiment Results

In this section, we present additional experiment results.

F.1 Experiments with Larger λ

All the experiments presented in the main paper are with $\lambda = 1$. In this subsection, we present results with $\lambda = 20$. See Figures 3 and 4 for results with MSE loss and CE loss respectively. The results supports our observation in the main paper that HERTA works consistently well on all settings.

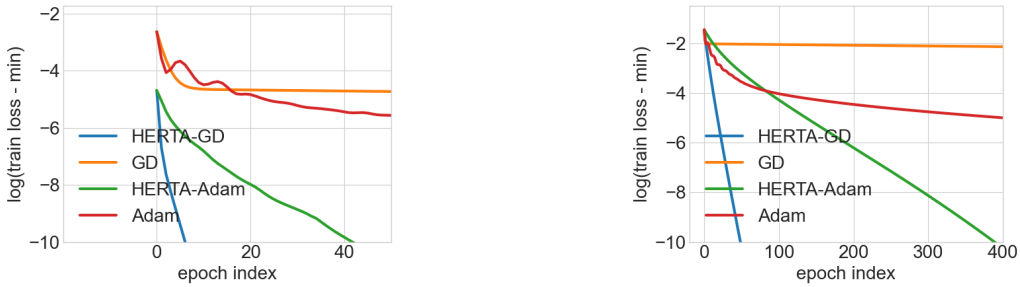

Figure 3: The training loss comparison between HERTA and standard optimizers on MSE loss with $\lambda = 20$. Dataset used from left to right: ogbn-arxiv, pubmed.

[3] https://pytorch.org/

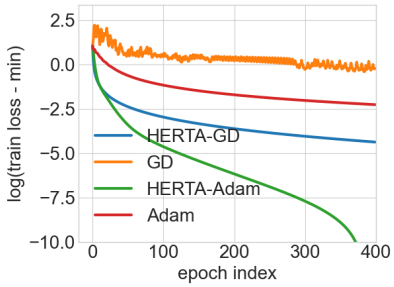

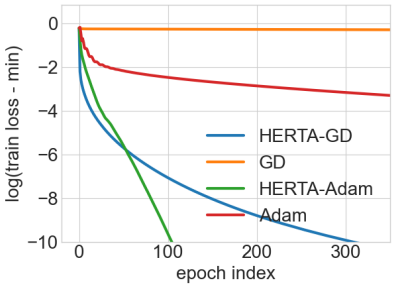

Figure 4: The training loss comparison between HERTA and standard optimizers on CE loss with $\lambda = 20$. Dataset used from left to right: ogbn-arxiv, pubmed.

F.2 Additional Results on Cora and Citeseer

In this subsection we present results on Cora and Citeseer, which are other citation datasets used in [46]. See Figure 5 and Figure 7 for results with $\lambda = 1$ and $\lambda = 20$ on Cora respectively. See Figure 6 and Figure 8 for results with $\lambda = 1$ and $\lambda = 20$ on Citeseer respectively. It is clear that the results on Cora is consistent with our observation on other datasets.

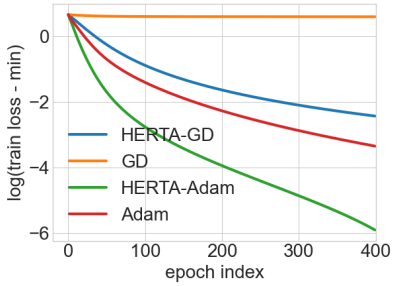

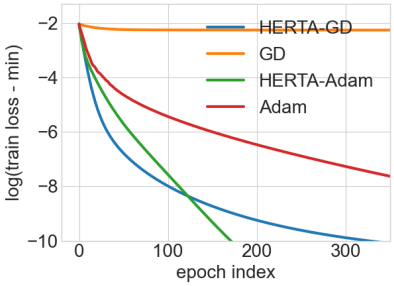

Figure 5: The training loss comparison between HERTA and standard optimizers on Cora with $\lambda = 1$. Left: CE loss. Right: MSE loss.

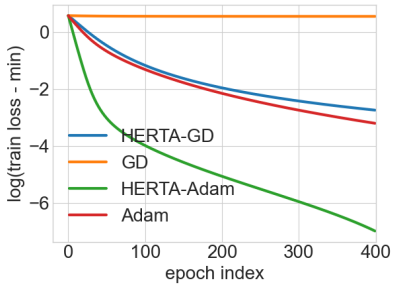

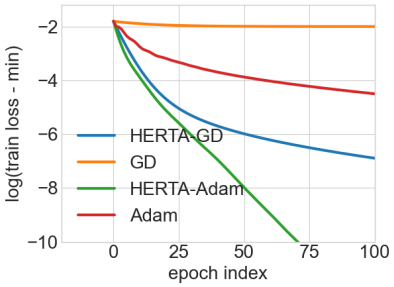

Figure 6: The training loss comparison between HERTA and standard optimizers on Cora with $\lambda = 1$. Left: CE loss. Right: MSE loss.

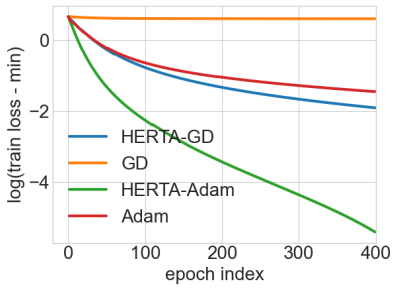

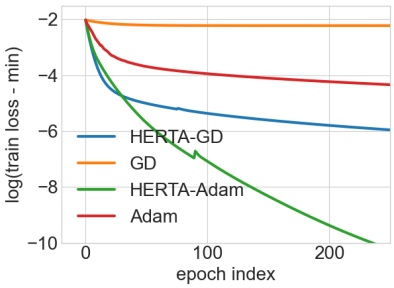

Figure 7: The training loss comparison between HERTA and standard optimizers on Cora with $\lambda = 20$. Left: CE loss. Right: MSE loss.

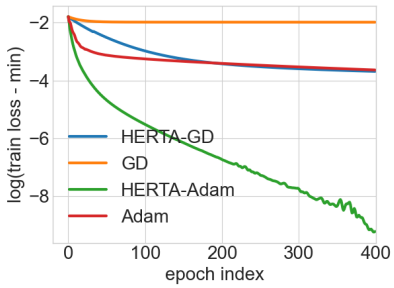

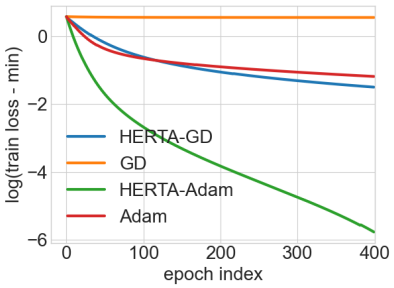

Figure 8: The training loss comparison between HERTA and standard optimizers on Citeseer with $\lambda = 20$. Left: CE loss. Right: MSE loss.